R-06-124

Numerical studies on spatial variation of the in situ stress field at Forsmark – a further step

Site descriptive modelling

Forsmark – stage 2.1

Hossein Hakami, Itasca Geomekanik AB

December 2006

Svensk Kärnbränslehantering AB
Swedish Nuclear Fuel
and Waste Management Co
Box 5864
SE-102 40 Stockholm Sweden
Tel 08-459 84 00
+46 8 459 84 00
Fax 08-661 57 19
+46 8 661 57 19

ISSN 1402-3091
SKB Rapport R-06-124

Numerical studies on spatial variation of the in situ stress field at Forsmark – a further step

Site descriptive modelling

Forsmark – stage 2.1

Hossein Hakami, Itasca Geomekanik AB

December 2006

Summary

The present work is an investigation into the depiction of a spatial distribution of the in situ stresses at the Forsmark candidate site. The methodology is based on numerical simulations of the pre-occurrences of perturbation of the stress field, produced by the deformations/ displacements that rock mass/major fracture zones undergo. The distinct element program 3DEC, /Itasca Consulting Group Inc. 2003/, was used for the purpose.

Forsmark area is dominated mainly by the Forsmark and the Singö faults but also by a number of major fracture zones. Almost all these structures, not only that they are reported to dip vertically, but they more or less run sub-parallel with the inferred overall orientation of the major principal stress, σ_1. These zones, as a result, cause a fairly limited perturbation in the state of in situ stress at the site.

At a diminished scale, however, fracture zones of a lesser extent – which dip obliquely and run at an angle in relation to the σ_1 orientation – produce a significant perturbation of the state of stress.

This work also included two preliminary investigations on:

– Assessing the remote orientation of the major principal stress. This was done by looking at the crustal shortening, which characterizes in part the past tectonic activities of the Fennoscandian shield.

– Looking for the mechanically viable explanations for the formation of joints sub-parallel with ground surface within the uppermost section of the rock mass.

Sammanfattning

Den här studien är en undersökning av den spatiella variationen hos in situ-spänningen i Forsmarks platsundersökningsområde. Metodologin baserar sig på numeriska simuleringar av variationer i spänningsfältet orsakade av deformation i bergmassan och förskjutningar längs de stora sprickzonerna. Till detta användes beräkningsprogrammet 3DEC /Itasca Consulting Group Inc. 2003/.

Området kring Forsmark domineras huvudsakligen av två förkastningar (Forsmark och Singö) men även flera andra större deformationszoner återfinns. De flesta av dessa strukturer, är inte bara rapporterade att stupa vertikalt, de är även mer eller mindre sub-parallella med orienteringen på den största huvudspänningen, σ_1. Detta innebär att dessa zoner orsakar relativt begränsade förändringar i spänningsfältet på platsen.

I en något mindre skala förekommer dock sprickzoner med en flack stupning och med en stryknning med viss vinkel till orienteringen av σ_1, vilka ger en tydlig förändring i spänningsfältet.

Denna rapport innehåller även två mindre sidostudier i syfte att:

– Studera den storskaliga orienteringen för den huvudsakliga huvudspänningen. Detta gjordes genom att titta på effekten av jordskorpans kompression vilken karaktäriseras av hur tektoniken för den Fennoskandiska skölden tidigare sett ut.

– Identifiera mekaniskt rimliga förklaringar för bildningen av sprickor sub-parallella med markytan i de övre delarna av bergmassan.

Contents

1 Background

Likewise for other candidate sites, the main objective for this project was to – through the numerical simulations – set up a virtual model of the Forsmark candidate site in three-dimensions, in which the most influential faults and fracture zones would take part. The model would incorporate the current state of in situ stress estimated for the close vicinity of the boreholes in which the measurements were carried out. Even though point wise in nature, the stress measurements at boreholes, not only provide detailed information, on the local state of in situ stress, but they also provide a measure of the tectonic forces that once prevailed at the site, and now are reflected in stress measurements as "locked-in" stresses.

The structure geological investigations at Forsmark area have shown that the area was exposed to an era of severe tectonic activities. Among the more obvious evidences, are the large finite bodies of rock mass in between Forsmark and Singö faults, the so-called "tectonic lenses". In situ stress measurements, because of the fact that they contain a large variability lend themselves to significantly different interpretations. Nevertheless, they tend to show the possibility that the in situ stresses at Forsmark site could be relatively larger than those for comparable areas.

Being made aware of the perhaps peculiar state of in situ stress at Forsmark site, it appeared appropriate to – apart from the core work that should include the setting up of a usual in situ stress model at the chosen area – extend the numerical investigations to also include:

1. A look at a much larger region, trying to relate the orientation of the tectonically-induced crustal shortening, presumed to have had occurred in the latest geological era, to a plausible but coarse state of stress via a numerical model. It was assumed that, through this approach, more appropriate boundary conditions would be selected for the main modelling area.
2. An attempt to come up with some viable explanation about the mechanics behind the formation of the pseudo-layered structure of the uppermost horizon of the crystalline rock at the site. Should we succeeded in doing this, the next step would be to see how this horizon of rock would influence the in situ state of stress right below.

Goals

– To see how the past tectonic activities (occurrences of bulk crustal shortening) relate to the assumed direction of major principal stress.

– To choose boundary conditions for the local model that is not necessarily identical with the far-field boundary conditions.

– To see if the whole process (regional as well as local) of evaluating stress field improves the agreement between the measured contra the computed fields

The present work was preceded by a preliminary study with a partly hypothetical nature by /Mas Ivars and Hakami 2005/.

2 Far field domain

2.1 Influences from the past tectonics of the region

Research into the structure geology of the Fennoscandian shield has revealed that the inferred direction of the crustal shortening, during the sequence of geological eras, has undergone significant change. Likewise the derived direction of the maximum principal stress has changed critically, see /SKB 2005/. According to this report, the inferred direction of the bulk shortening very closely coincided with the N–S direction for 1,910–1,750 million years ago, see Figure 2-1, and then changed to E–W direction for 1,275–900 million years ago, see Figure 2-2.

The derived direction of the major principal stress, however, is seen to have undergone a dramatic change, from almost N–S (NNE–SSW) direction to a NW–SE direction, see Figure 2-3.

In Figure 2-3 the inferred orientations of the major principal stress are shown. Whereas the direction was roughly NNE–SSW for 95 to 60 million years ago, it rotated to align itself with a NW–SE direction.

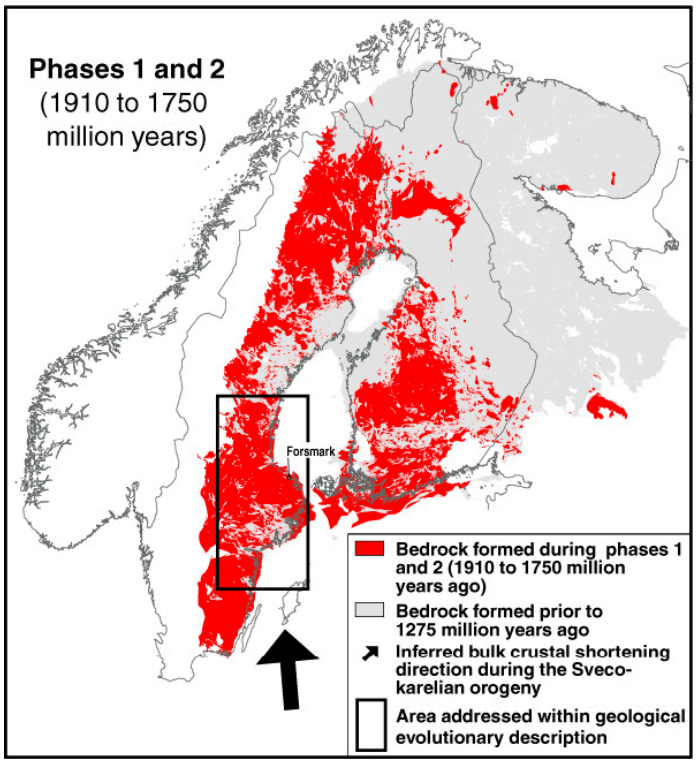

Figure 2-1. *The direction of crustal shortening in the area from 1,910–1,750 million years ago, it is close to N–S /SKB 2005/.*

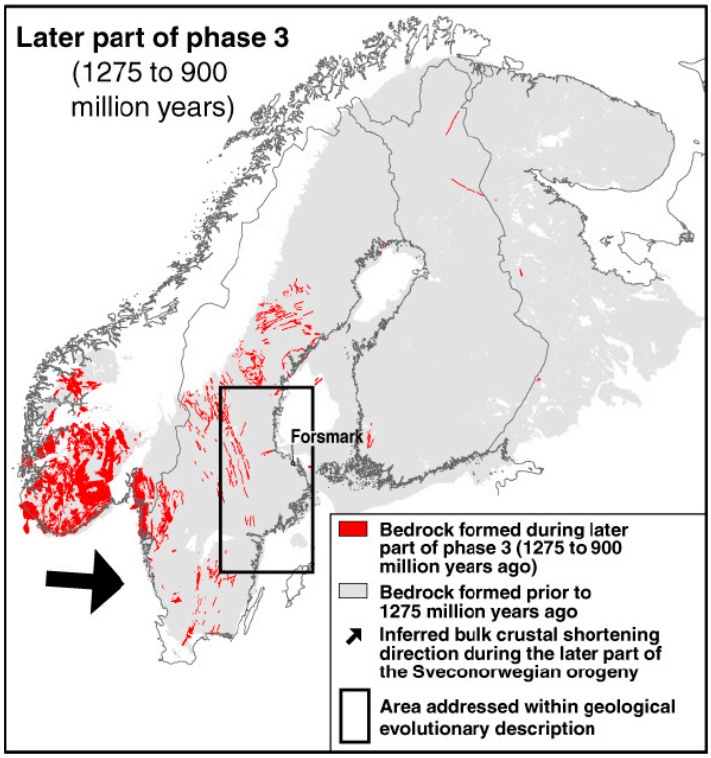

Figure 2-2. *The direction of the crustal shortening in the area from 1,275–900 million years ago, it is almost E–W /SKB 2005/.*

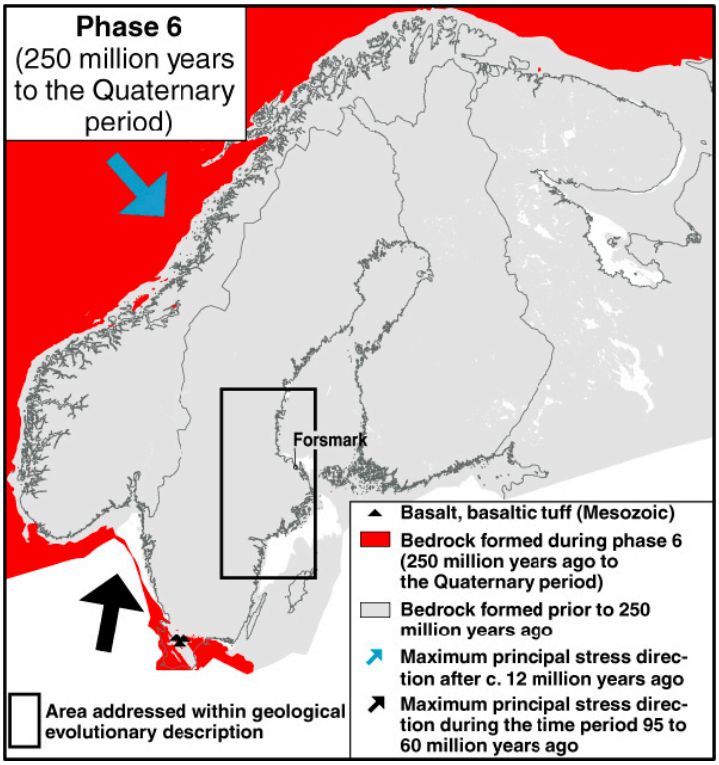

Figure 2-3. *The inferred orientations of the major principal stress from 250 million years ago to Quaternary period, it was about NNE–SSW during the period 95–60 million years ago and NW–SE after 12 million years ago /SKB 2005/.*

2.2 Numerical modelling approach

It was conceived informative to set up a numerical model, in which crustal shortening would be simulated. This could provide us with a numerically-inferred orientation of the major principal stress and, as a result, a basis could be made on which a comparison was made with the range of orientations for σ_1 inferred from in situ stress measurements. Besides, the findings would enable a more appropriate choice of boundary conditions for the main simulation area, see Figure 2-4 and also under Chapter 4.

Figure 2-4 shows a structure geological map of the area /SKB 2006/, based on which the numerical model was constructed.

Not only the brittle fracture zones, indicated on the map as BZ, were considered in setting up the numerical model, but also the less-investigated ductile zones were also included in the model. The possible paths of the ductile zones were chosen to approximately coincide with the central core of the wide tracks, marked out as ductile zones. Theses are indicated by DZ on the map.

Figure 4-1 was also used as a base map in order to include the selected fracture zones into the far-field model. Adding of the fracture zones named was made with the help of the coordinates of a selected number of points on each fracture zone extracted from the RVS-data base.

Figure 2-5 shows the model block, including all the fracture zones/faults selected. The network of the planar discontinuities, representing the fracture zones/faults in the model, may seem to be more complicated than it should be. This is because the segments of a fracture zone that remains passive; i.e. do not enter the computations, are also visible on the model block.

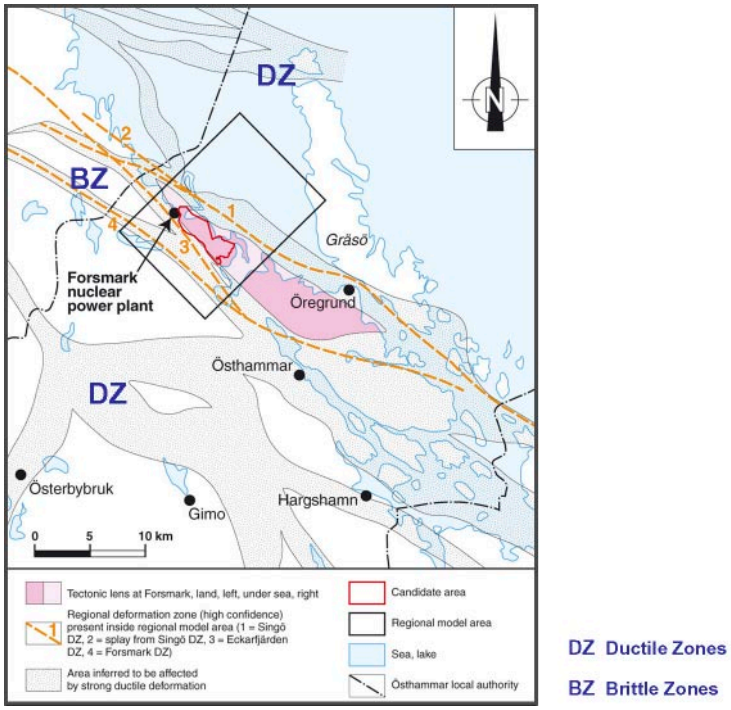

Figure 2-4. *Structure geological map over Forsmark. The rectangle, the so-called regional model shows the area on which the numerical model was based, /SKB 2006/.*

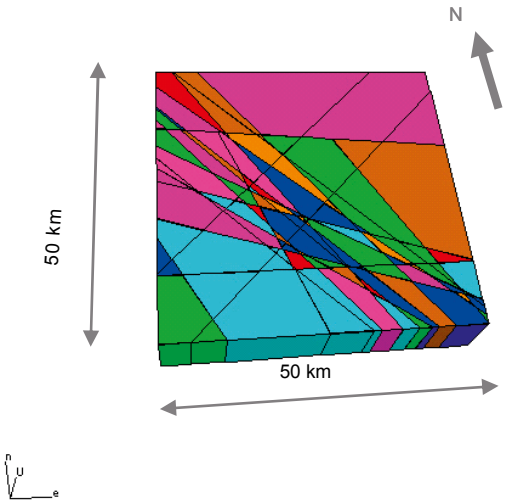

Figure 2-5. *The numerical block model used in simulations of the far-field domain.*

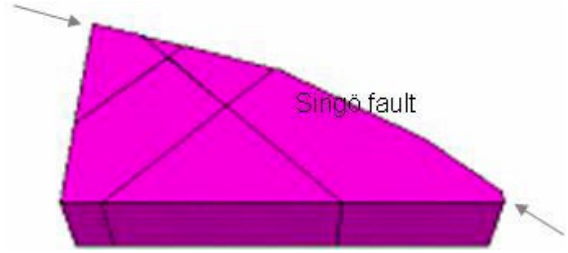

Figure 2-6. *Singö fault consisting of 3 segments to approximate the curvature of the fault in the numerical grid.*

Two major faults, namely the Forsmark and the Singö faults dominate the region by their distinctive characteristics, among others, the pronounced curvature along their momentous extents and the vastness of their size. The way the curvature of such fracture zones was taken into account in the numerical grid is shown in Figure 2-6. The fault shown is the Singö fault.

Figure 2-7 shows the block of rock mass confined between the Forsmark and the Singö faults. Ekarfjärd fault is also shown on the figure. A portion of the limits of the regional model is left on the figure for the ease of locating the rhomboidal block position in the model block. The rhomboidal block represents an important volume of the rock mass within the model block, as it contains the tectonic lenses and is the bedrock on which the Forsmark nuclear power plant is constructed.

The other fracture zones that were included in the model are shown on the map in Figure 4-1.

The inclusion of each of the fracture zones was made with the help of the coordinates of a selected number of points, made available by the geology section, extracted from the RVS data base.

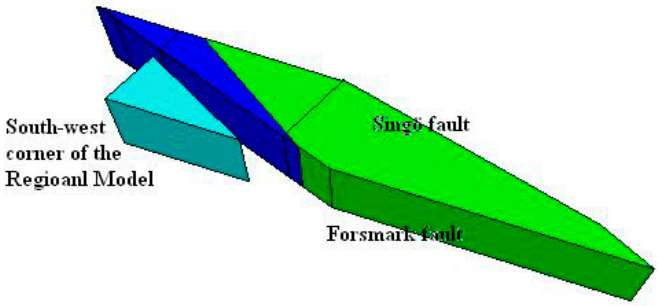

Figure 2-7. *Rhomboid made of Forsmark and Singö faults containing the tectonic lenses and where the Forsmark nuclear power plant is located. A portion of the regional model is also shown in the figure for the ease of positioning the rhomboid.*

2.3 Model specifications and simulation procedure

It was assumed that the rock mass, excluding all discontinuities distinctly incorporated in the model block, was elastic with the equivalent properties:

E (Modulus of Elasticity) = 40 GPa
ν (Poisson Ratio) = 0.24

All discontinuities modelled assumed to behave elasto-plastically, following the Mohr-Coulomb criterion of failure. The mechanical properties assigned to the discontinuities were:

Friction angle = 20°
Shear stiffness = 1×10^9 Pa/m
Normal stiffness = 0.5×10^9 Pa/m
Cohesion = 0 Pa

Boundary conditions for the numerical runs were:

- The top of the model, i.e. the ground surface, was made free from any restraints.
- The bottom of the model could be displaced in E–W direction but not in the vertical direction.
- The two walls at right angle to N–S direction could displace in E–W direction but not in N–S direction.
- The two walls at right angle to E–W direction were set to move inwards at a low, constant velocity.

Under the above boundary conditions, a number of numerical simulations were made in which the runs were terminated when the major principal stress, σ_1, at a depth of 500 m reached about the values the in situ stress measurement in the area had indicated. A record of the variation of the trend of σ_1 for each run was then made.

2.4 Results

Figure 2-8 shows the principal stresses within the rhomboidal sub-block. The three orthogonal bars symbolize the major, the intermediate and the minor principal stresses.

In Figure 2-9, the periphery of the regional model and the in situ stresses inside are also added to the rhomboidal sub-block. Boundary conditions in form of surface tractions, concluded from the far-field model analyses were meant to be applied to the regional model boundaries, see under Chapter 4. However, because of the many simplifications made in setting up the model and the lack of knowledge about the current direction of crustal shortening at the area, the inferred range for the orientation of σ_1 compared poorly with the same range obtained through in situ stress measurements.

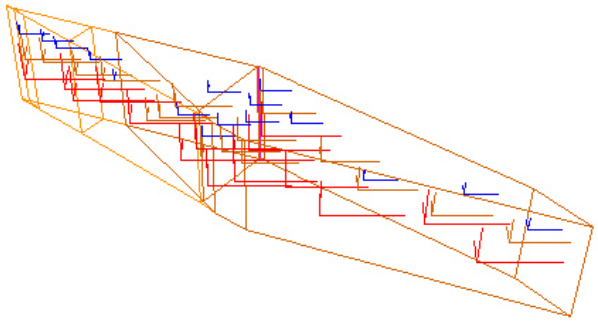

Figure 2-8. *The Forsmark rhomboid inside which a selection of the in situ principal stresses are visualized; the stresses shown were produced at the end of a numerical run in which the crustal shortening was simulated.*

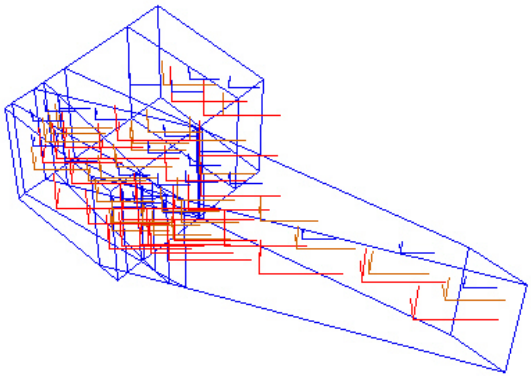

Figure 2-9. *The regional model and the Forsmark rhomboid; a range of the orientations of σ_1 was chosen to define the stress tractions on the relevant boundaries of the regional model.*

3 PFC analyses

At Forsmark there exists a pseudo-layered top rock cover, divided by a number of the so-called sheet joints, which is not a usual occurrence. Apart from the impact it may have on the hydrology/hydrogeology of the area, it is suspected that the structure also plays a role on the state of the in situ stress at that area. Probing into the basic causes for the emergence of such structure is deemed desirable as it hopefully may give us some clues on how it would have affected the in situ state of stress at the site.

3.1 Aim

The aim of this work was primarily to come up with a conceptual model – through numerical analyses – that would describe the mechanics behind the emergence of such structure. Should the conceptual model appear plausible, the next task would be to infer information that relates to the state of stress at the site.

The conceptualization is based on two premises:

– A semi-detached discontinuity runs below the top rock cover containing the sheet joints.

– A preferred orientation at the grain size level should have occurred in the top rock cover during the micro-tectonic activities associated with the formation of that rock.

3.2 Model set-up

The program Particle Flow Code, /Itasca Consulting Group Inc. 2004/ was used for the numerical simulations. A large number of particles, shaped as circular disks, were placed inside a beam-like rectangle that formed the outline of the model. A semi-detached discontinuity, running at mid-depth of the beam, included as many particles as their centroids could fall inside an interface of known thickness. Up to three weakness planes, denominated as “Preferred Orientations”, including only one row of particles ran parallel with the semi-detached discontinuity. These were to simulate the assumed alignments of rock grains/crystals, which later would facilitate for the sheet joints to form.

Figure 3-1 shows the geometry of the model. The chosen dimension of the model was 2,000 m×476.5 m. As the model was just conceptual, the findings could apply to any model with a size of many folds larger as long as the ratio width/length was kept constant.

The bottom of the model was conditioned such that no movement was allowed in the y-direction. Movement in the x-direction, however, was made possible. The top of the model was made free from any restrictions in order to resemble a traction-free rock surface.

The vertical boundaries were conditioned to behave in two ways:

I) Inward movement of the model vertical walls with a constant velocity in the horizontal direction. This was meant to resemble a superficial crustal shortening.

II) Inward movement of the model vertical walls as above including a rotational component at the points shown. This was thought may also offer a plausible deformation of uppermost thickness of the earth crust.

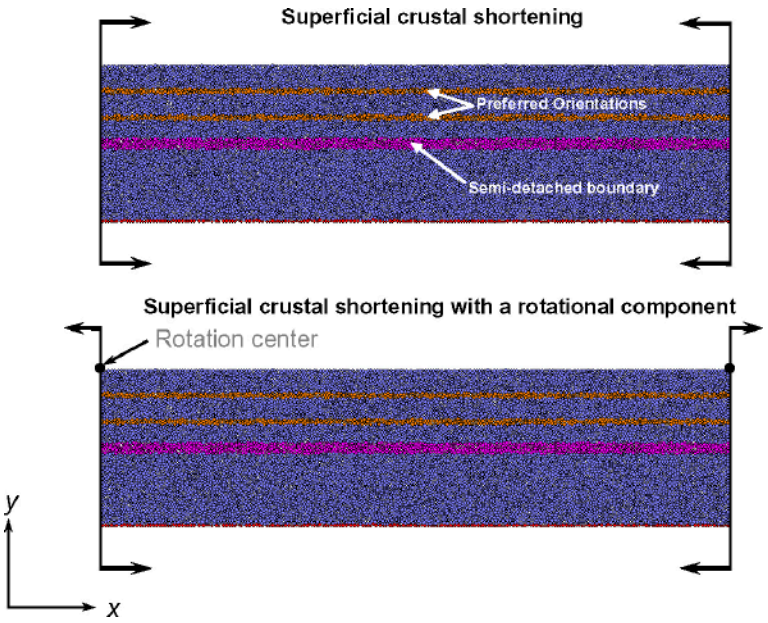

Figure 3-1. *Configurations of the PFC-models showing the semi-detached boundary, the preferred orientations and modes of deforming the rock beam; Mode I (above), purely translational and Mode II (below) including a rotational component.*

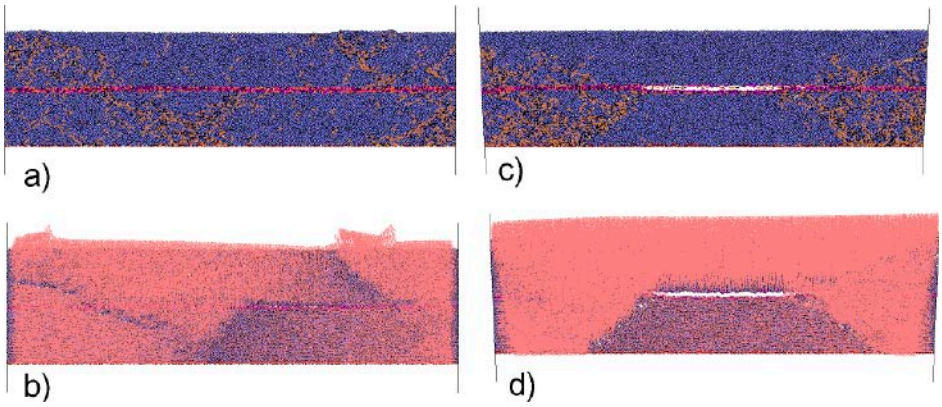

Figure 3-2. *Fracture propagation and the displacement vectors in the absence of the preferred orientations, a) and b) in Mode 1 of deforming the rock beam. Likewise are c) and d) in Mode II of deforming the rock beam.*

To begin with a number of analyses were performed where the preferred orientations were excluded from the model, see Figure 3-2. The pattern of crack propagation in both deformational Modes I and II was, in principle, similar. Swarms of conjugate cracks were developed. The cracks ran angled, 40–45 degrees, in relation to the horizontal axis. Whereas in Deformation Mode I the crack network seemed to have more spread over the entire model, a clear separation in the middle of the semi-detached boundary was formed under Mode II. Two distinct swarms of cracks tend to have connection to the endpoints of the separated section.

Displacement vectors tend as well to have been influenced by the presence or the lack of the separated section along the semi-detached boundary. In Deformation Mode I, the more pronounced fractures emerging from the crack swarms break through the ground surface whereas this did not take place in Deformation Mode II.

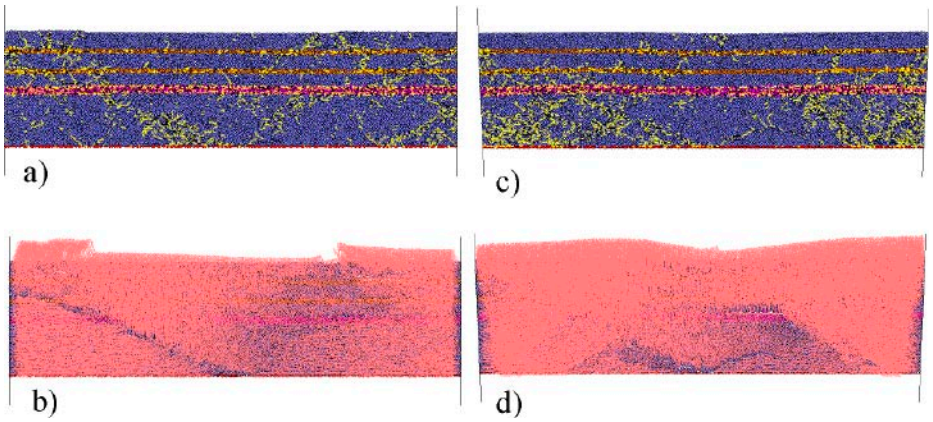

Figure 3-3. *Fracture propagation and the displacement vectors in presence of the preferred orientations, a) and b) in Mode 1 of deforming the rock beam. Likewise are c) and d) in Mode II of deforming the rock beam.*

In the next series of analyses, the preferred orientations were made available in the model, see Figure 3-3. In Deformation Mode I, the separated section tends to diminish in extent and the swarms of conjugate cracks appear to have a wide spread, not only in Deformation Mode I but also in deformation Mode II. A number of cracks align themselves with the preferred orientations creating open fissures along those weak planes.

As the modelling of the tectonic activities, i.e. the crustal shortening was done with over-simplifications, it is difficult to choose any of the two deformation modes described as more conceivable. Yet a visual comparison with the structure geological maps of subarea in question favours the Deformation Mode I, in which the rotational component was not present.

The study supports the assumption on the sequence of the tectonically-induced fracturing that sheet joints emerged following the formation of the oblique fractures/fracture zones.

The fact that the oblique fractures/fracture zones in numerical simulations extended beyond the semi-detached boundary of the model implies that they have far more influence on the spatial distribution of in situ stresses at greater depths. Sheet joints presumably should have substantially distressed the top rock cover within its extent. Therefore its effect on the state of stress below could hardly be more than that expected from a dead weight.

4 In situ stress field at Forsmark – a regional model

4.1 Geometrical lay-out

The structure geological modelling area, defined as the regional model, see /SKB 2005/ was used as the basis for laying out the geometrical structure of the numerical model, set up by the distinct element program 3DEC, /Itasca Consulting Group Inc. 2003/. Faults and the majority of the fracture zones, crossing over the limits of the regional model were incorporated into the geometrical framework of the numerical model, see Figure 4-1. The discontinuities were simplified in shape to planar surfaces, which later could be assigned with appropriate mechanical properties.

Site investigations so far carried out at Forsmark confirm that the majority of the major discontinuities – at least down to the depths over which site information could be collected – dip close to vertical. Further more, a range of ± 10° from the vertical have been assumed as a possible range for the occurrence of the discontinuities. In the absence of any more specifications the faults/fracture zones incorporated in the numerical model were assigned a dip of 90°.

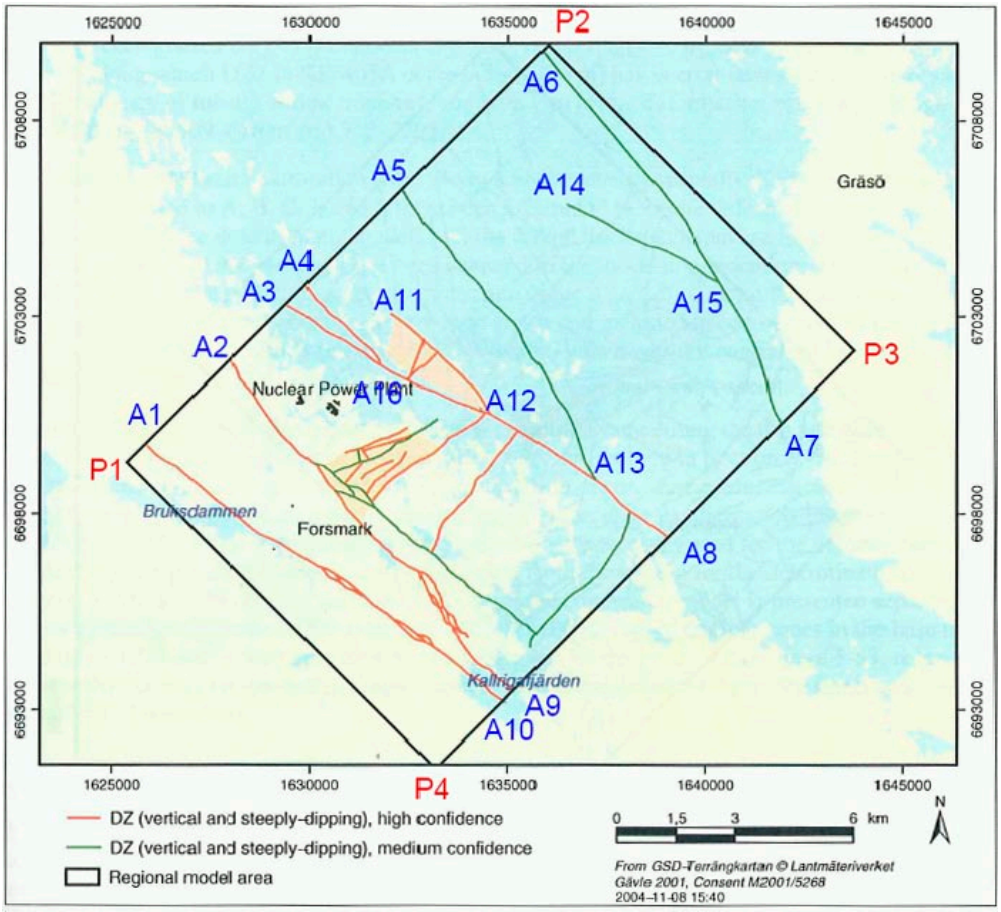

Figure 4-1. *Structure geological map showing the discontinuities that were incorporated in the numerical model; the regional model, see /SKB 2005/, as marked by points P1 through P4, was covered identically by the numerical grid.*

Figure 4-2 shows the numerical model block. The uppermost 350 m of the model block was removed in order to conform the model block to accumulate the stress field given under Section 4.2.

The dimensions of the horizontal cross section of the model block measured to 11×15 km. The model was made 7 km in depth even though the data collection covered just to a depth of less than a kilometre. The choice of a great depth as such was to prevent the numerical model from any boundary effects and a possible rotation of the model block.

Of the fracture zones intersecting the rock mass in between the Singö fault, Eckarfjärden fracture zone and the Forsmark fault, ZFMNE0065 and ZFMNE00A2 were included in the numerical model block. These fracture zones lay within a well site-investigated subarea with a fairly high frequency of occurrence of similar fractures – although less dominant, especially those nearly-parallel to ZFMNE00A2, see Figure 4-4 and Figure 4-5. A comparison between the stress distribution pertaining to this subarea, inferred from site investigations vis-à-vis numerically determined could point to the appropriateness of the numerical model or to the contrary.

Figure 4-3 is a simplified sketch of the numerical model block that shows the forking of two major discontinuities into splays. A planar surface representing a splay in the 3DEC model was made active in computations just over its real size.

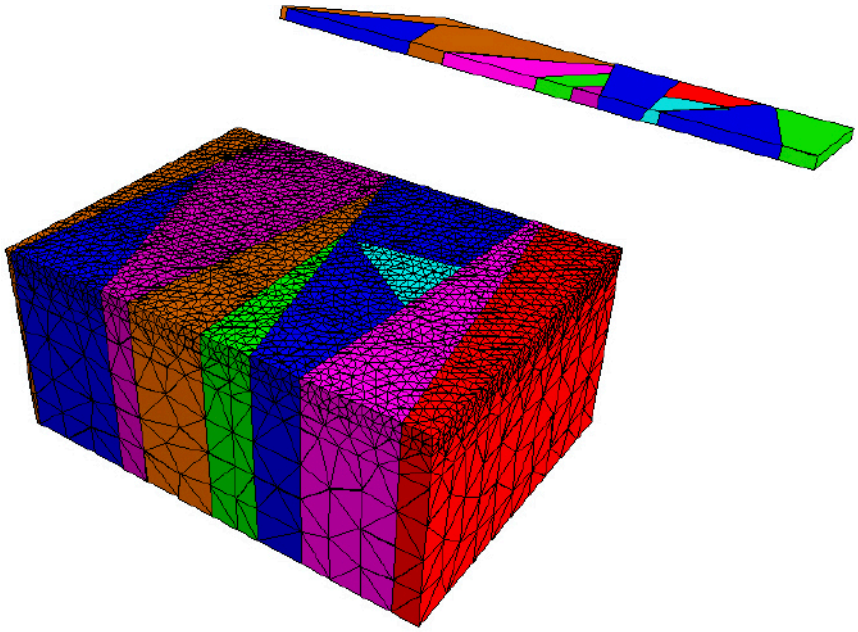

Figure 4-2. *The discretized model block showing also the calculation tetrahedral. The uppermost section, 350 m in thickness, was removed in order adjust the computations to comply with the range of the validity of the in situ stress evaluations.*

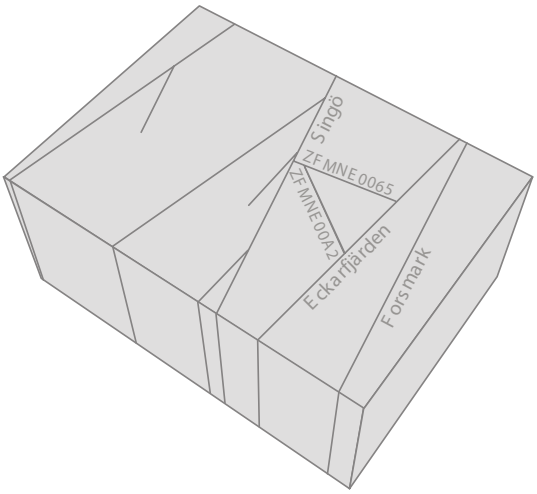

Figure 4-3. *A simplified sketch over the numerical model block shown in Figure 4-2.*

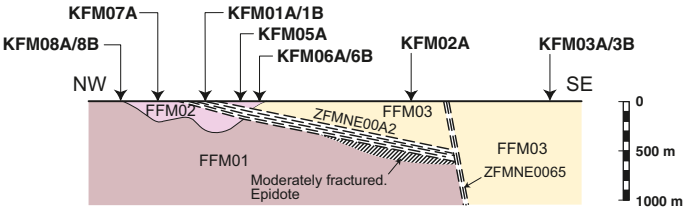

Fracture domain FFM01
Steeply dipping, minor fracture zones with sealed fractures, low fracture frequency between zones, high in situ stress

Fracture domain FFM02
High frequency of sub-horizontal fractures with apertures

Fracture domain FFM03
High frequency of gently dipping, minor fracture zones containing both sealed fractures and fractures with apertures, low in situ stress relative to FFM01

Figure 4-4. *Sketch made on a vertical section, delineating fracture domains with different characteristics. Fracture zones ZFMNE00A2 and ZFMNE0065 act as the border lines between the different fracture domains, /SKB 2006/.*

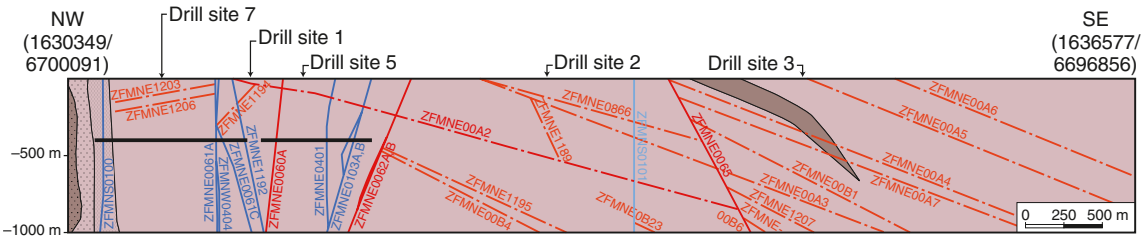

Figure 4-5. *Fracture pattern on a NW-SE vertical section, /SKB 2006/. Note the fracture zones nearly-parallel to ZFMNE00A2. These fracture zones, in similarity to the fracture zone ZFMNE00A2, contribute to important variations in the local state of the in situ-stresses.*

4.2 In situ stress field

In Forsmark, despite the extensive in situ stress measurement campaigns, the evaluations so far have not resulted in a non-disputable picture of the stress field. The difficulty lies in the fact that the variation in measurement results is very significant. In particular the uncertainty associated with results from the top 350 metres of the bedrock is very large to the degree that the values have been excluded from the rest of the measurement results under evaluations. The expressions thus being put forward yield the variation of the principal stresses beginning from a depth of 350 m and ending at the depth of 650 m. The tentative expressions see /SKB 2005/ yielding average values, read as below:

$$\sigma_H = 35 + 0.020Z \quad (1)$$

$$\sigma_h = 19 + 0.025Z \quad (2)$$

$$\sigma_v = 0.026Z \quad (3)$$

The average orientation of the maximum horizontal stress, σ_H, was given to be N140°.

The above expressions were incorporated into the numerical models to define the initial stress field within the regional model. When the expressions 1–3 were used to define the tractions on the boundaries of the regional model, just a limited sub-range (130°–140°) from the wider range of orientations for the major principal stress in Sweden was taken into consideration. /Sjöberg et al. 2005/ give an account of the possible ranges for the orientation of σ_H measured at different sites in Sweden, from which it may be seen that a range of 120°–150° would encompass all the values reported.

4.3 Mechanical properties of the model constituents

4.3.1 Mechanical properties of the rock mass

In this work, by rock mass it is meant the rock volumes that exist outside the discontinuities, which were included in the numerical model distinctly. The rock mass as such was treated as an equivalent continuum. From the earlier investigations with the aim to determine the equivalent properties of the rock mass at Forsmark /SKB 2005/, calculated range of values for the modulus of elasticity, E, equal to 40–80 GPa and the Poisson ratio, ν, equal to 0.20–0.35 had been estimated. For the numerical analyses, values of E = 40 GPa and ν = 0.24 were chosen. The constitutive criterion chosen for the modelled rock mass was Mohr-Coulomb.

4.3.2 Mechanical properties of fracture zones

Faults and fracture zones as found in the geological formations are indeed very complex structures and their deformational behaviour has been a subject for research for decades. Attempts to represent them in a numerical model necessitate gross simplifications. It is, therefore, important to note that the mechanical properties assigned to those structures in a numerical model differ significantly from the values that may normally be obtained in the laboratory on small samples of rocks. To make a clear distinction, the values chosen here to define the different mechanical properties pertaining to the modelled discontinuities will be named as *apparent mechanical properties*. A magnitude appearing under an apparent property may not even be reasonable in a physical sense.

Splays with free ends inside the model block – even though their representative planar surfaces ran through the periphery of the model block were made active just over the lengths in question, see Figure 4-4. In the same manner, all of the discontinuities modelled were active down to 2,000 metres and deeper down they were made as passive entities.

The way the mechanical properties were assigned to the geological structures modelled was to consider that larger fracture zones could mobilize lower frictional resistance against shearing and were less stiff because of a wider zone of influence. Some of the deformation zones the occurrence of which was classified by a *medium confidence´* were not chosen to include in the numerical model. The other zones in this category, which entered the numerical model, received the same properties as for the zones determination of which had been made with a *high confidence*.

Table 4-1 summarizes the magnitudes assigned to the discontinuities modelled.

4.3.3 Boundary conditions

The vertical limits of the model block were loaded with stresses according to the expressions 1–3 (see Section 4.2). The bottom boundary was set such that no displacement could take place in any directions.

Because of the lack of reliable in situ stress measurements data at shallow depths at the time a depth range of 350–650 m had been set as the upper and the lower limits of the validity of the expressions 1–3. The very low gradients were presumably the result of a regression analysis on not all but a sensible selection of data points from the depth interval mentioned.

Accordingly, it was judged as appropriate to remove the uppermost 350 metres of the rock from the numerical model block. As a substitute for this removal the upper boundary, which now laid at a depth of 350 m, was loaded with a traction equivalent to the weight of the rock removed.

4.4 Results

A number of analyses were performed in order to reproduce numerically the spatial distribution of in situ stresses at the area in question. The majority of the analyses were purposed to help understanding the sensitivity of the results with regard to the input parameters chosen.

As could be anticipated, because of the fact that the range of orientations for the major principal stress which were accounted for in the numerical simulations made a very low angle to the majority of the discontinuities modelled and that the discontinuities ran vertically downwards into the bedrock, just very small shear displacements could be produced by the change in the prevailing *in situ* stresses. As a consequence of this, just marginal disturbances in stress field could be detected close to the discontinuities.

The distribution of in situ stresses within the area containing the fracture zones ZFMNE0065 and ZFMNE00A2, however, exhibited a significant variation. This was expected as the discontinuities dipping at low to medium angles (roughly 25°–75°) create an important redistribution of the stress field in their neighbourhood. Figure 4-6 shows the major principal stress, σ_1, close to a horizontal section taken at a depth of 400 m.

Table 4-1. The magnitudes assigned to the modeled discontinuities.

Discontinuity	Friction angle [°]	Normal stiffness [Pa]	Shear stiffness [Pa]	Cohesion [Pa]
Regional through-going fracture zone/fault	20	1×10^{9}	0.5×10^{9}	0
Large fracture zones/ splays with limits inside the modelled area	25	1×10^{10}	0.5×10^{10}	0

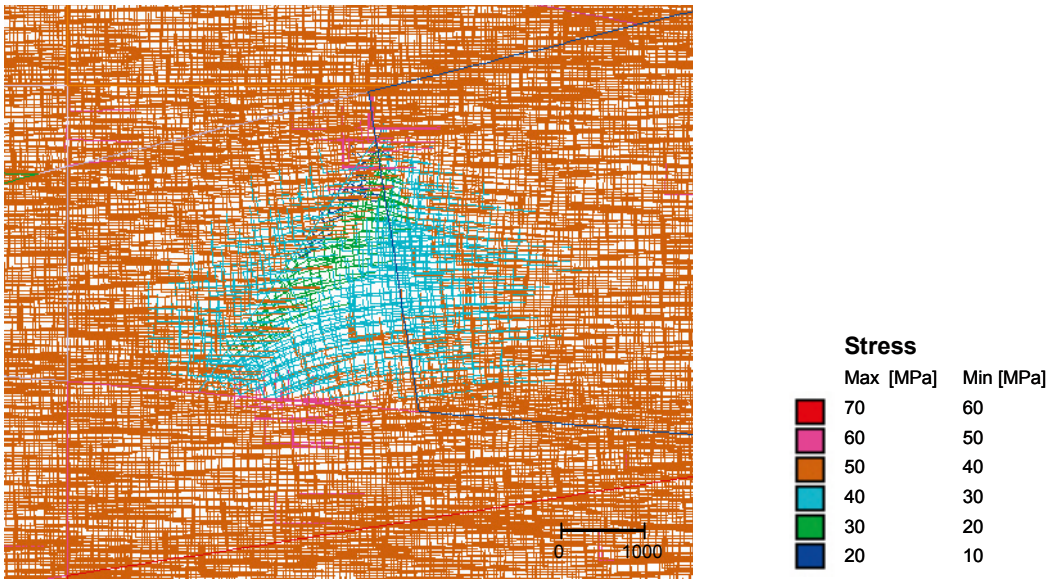

Figure 4-6. *A horizontal section at the depth of 500 m through which the computed major principal stress, σ_1 occurring in the close vicinity of the section are sighted.*

In the area delimited by the ZFMNE0065, ZFMNE00A2, Ekarfjärden fracture zones and in the vicinity, not only a notable deviation of σ_1 trajectories is seen but also a reduction in the magnitude of that stress is noted.

Figure 4-7 is a vertical section through the area that mirrors the vertical section in Figure 4-5. The nearby principal stress tensors are seen through the vertical cross section. A comparison with the qualitative information on the state of in situ stress indicated on Figure 4-4 verifies the correctness of the loading/unloading occurrences in the area.

In order to show the variation in magnitudes, trends and plunges of the principal stresses within the model block, data were collected along nine profiles. These profiles are indicated in Figure 4-8 and include:

b) Three profiles oriented in N–S direction at the depths of 400, 500 and 600 metres.

c) Three profiles oriented in the E–W direction and at the depths of 400, 500 and 600 metres.

d) One vertical profile at the intersection between N–S and E–W profiles.

Figure 4-9 to Figure 4-11 show the major principal stresses along E–W scan lines running at 400, 500 and 600 m deep. Significant variation in the magnitude of the stresses takes place around the intersection of the scan line with ZFMNE0065 and ZFMNE00A2.

Data on the magnitude and the orientation of the major principal stresses, collected along all the scan lines represented in Figure 4-8 are given in Appendix 2.

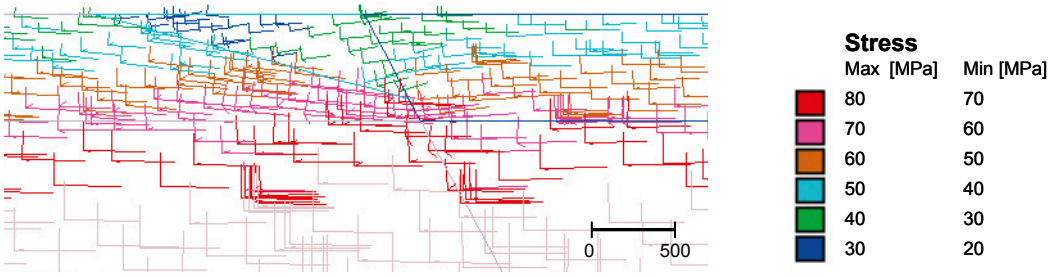

Figure 4-7. *A NW–SE vertical section (see also Figure 4-5) through which the nearby principal stress tensors can be sighted. Note the rotation of the tensors in passage over ZFMNE0065 and ZFMNE00A2.*

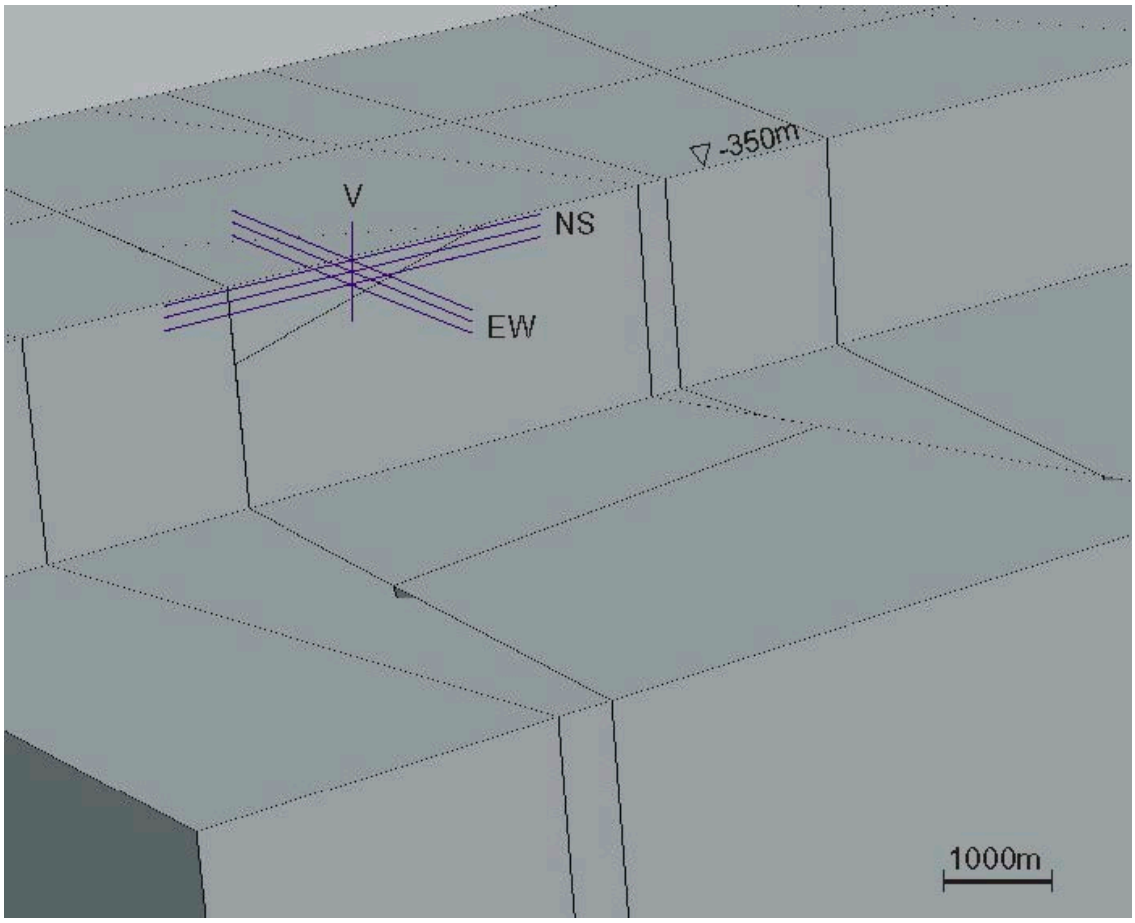

Figure 4-8. *In the model stress, trend and plunge were measured at three different depths; 400, 500 and 600 metres. These measurements were made at six different scan lines; three in the direction N–S (northing) and three in E–W (easting). Where the N–S and E–W scan lines intersect (at different depths) a vertical scan line was measured between the depths 400 and 820 m.*

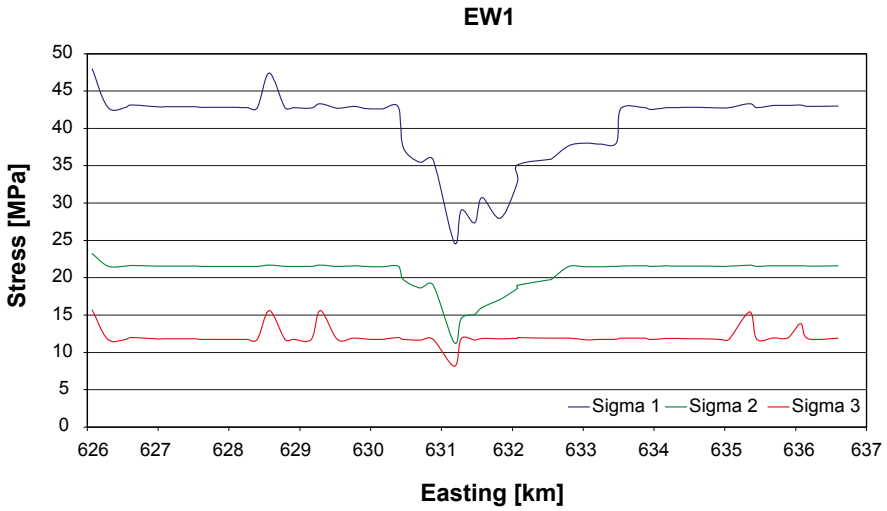

Figure 4-9. *Variation of σ_1, σ_2 and σ_3 along E–W scan line at 400 m depth.*

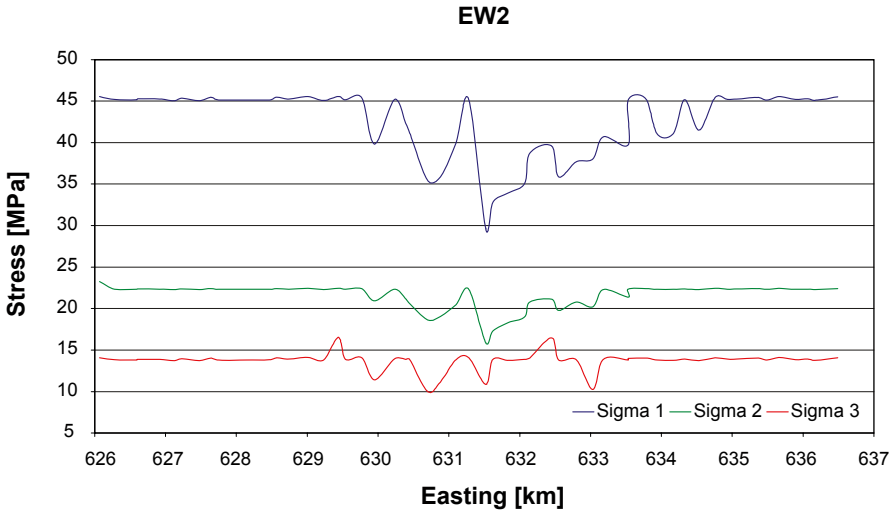

Figure 4-10. *Variation of σ_1, σ_2 and σ_3 along E–W scan line at 500 m depth.*

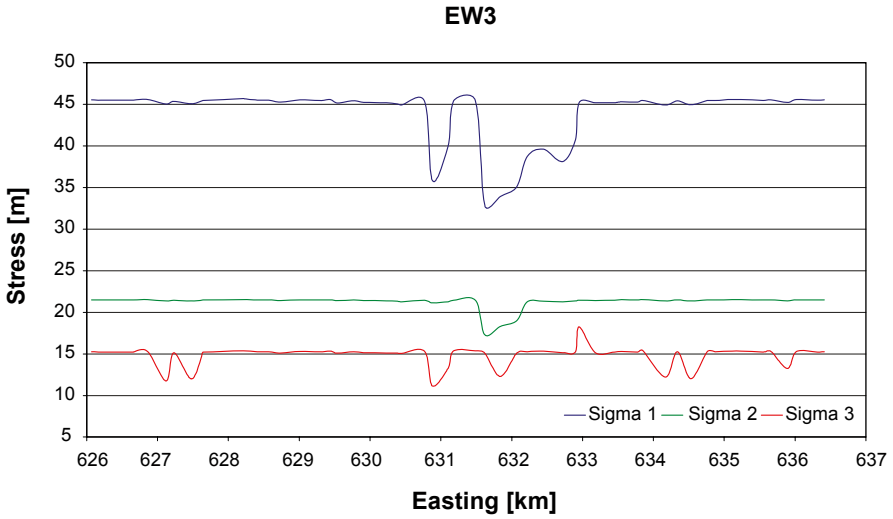

Figure 4-11. *Variation of σ_1, σ_2 and σ_3 along E–W scan line at 600 m depth.*

5 Discussion

Even though the results from the numerical investigations for the far-field domain delivered a useful but rough evaluation of the spatial distribution of the in situ stress field, it could not convincingly limit the span of uncertainties associated with the orientation of the major principal stress, σ_1, in the subareas of interest. This is because the uncertainty associated with the direction of the crustal shortening is high. The boundary conditions, which for the regional model, i.e. stress tensors deduced from the analyses pertaining to the far-field domain, would, as a consequence, involve roughly the same span of uncertainty emerging from the far-field analyses. It is then disputable whether or not a regional model, steered primarily by the direction of crustal shortening, would contribute in setting up more accurately-oriented boundary conditions for the regional model.

A positive aspect of simulations at the far-field domain, though, is that major faults and fracture zones, which normally bend at some points along their stretches, participate in the model with greater lengths, some possibly at full lengths, in the simulations. In contrast a truncation of the very large discontinuities should be done in a smaller scale model, here the regional model, to confine them to the size of the area in question.

The simulations by Particle Flow Code in two dimensions indeed shed some light on the mechanics behind the formation of the top rock cover at the top with an internal pseudo-layered structure. The formation of the oblique shear bands, out of which conjugate fractures further would emerge, followed by the alternated creation of open flaws along the "preferred orientations" tend to show that the assumptions on which the numerical grid was built were plausible. The simple mechanics, which underlay the set-up of the numerical model, namely that the pseudo-layered structure at the top was a production of a flexural bending (simple bending in two-dimensional) due to the tectonic forces appears viable.

Despite the indications on the viability of the mechanics described, it did not turn out to be apparent, from the outcome of the limited investigation carried out, how the link between the top rock cover and the rock mass below should be established. A plausible link could be a vertical stress transfer, which corresponded to the weight of the overburden – keeping in mind that the top rock cover should mainly be distressed horizontally. The question of how the top rock cover could have affected the in situ stresses at the area remains to be further investigated. It is also to be remembered that the PFC-analyses were two dimensional, and should be extended to 3 dimensional in order to comply with the 3DEC-analyses performed.

It is interesting to note that the direction of the crustal shortening, once at about a right angle to the strike of the most dominant faults, which assumingly later emerged, namely the Forsmark and the Singö faults, undergo a dramatic change in a next geological era and runs roughly parallel with the strike of the faults mentioned. Once prevailing in this direction, the crustal shortening neither could produce significant displacements across the named faults nor across the other major fracture zones, whose strike occur to make just small angles with that most recent direction of the crustal shortening. The results from the 3DEC analyses pertaining to the so-called "regional model" are very much in line with the idea given i brief above. Similarly, the displacement inferred from the 3DEC-analyses tended to be limited in size. Consequently the disturbances on the in situ stress field were, at the scale of the area studied, small. The in situ stress measurements carried out so far tend not to depict a more comprehensible picture of the stress field at the Forsmark area. Apparently the occurrence of the numerous fracture zones of minor intensity but at low inclinations, which exist in the area are responsible for the significant variation of the in situ stresses, being inferred from the stress measurements. Local models that cover a selection of subareas at limited sizes, preferably enclosing measurement boreholes, are then to be erected to verify the postulation that the Forsmark site may include subareas that secure more elevated in situ stress.

6 Conclusions

The simulations of the in situ stress field at Forsmark – at the scale relevant to the "regional model" in this study – do not capture any occurrence of unusually-loaded subarea.

The numerical model set-up reflects greater sensitivity to the scale and the orientation of the regional discontinuities than to the variations in the supply of mechanical properties to those structures.

Borehole-based evaluations of the in situ measurements should be enhanced in order to justify the enlargement of the numerical block, as constructed in this work, to reach the ground surface.

The majority of the major fracture zones/faults at Forsmark are nearly parallel with or make a small angle to the orientation of the major principal stress, σ_1. This clarifies why the corresponding disturbances in the in situ stress field are minimal.

A significant re-distribution of the in situ stress field took place within and around the rock wedge made in part by the fracture zones with low to medium inclinations, i.e. ZFMN00A2 and ZFMN0065, with low to medium inclinations.

The study with the Particle Flow Code, as an attempt to understand the mechanics behind the formation of sheet joints in the uppermost rock (rock cover) appeared informative. However, as long as load transfer is concerned, a link between the top rock cover and the rock mass below could not be established.

The far-field simulations are informative as long as they help setting up more enhanced boundary conditions for any subarea from the whole domain. Yet the very large scale of the rock covered by the numerical model masks the local occurrences of significant variations in in situ stress field because of an outstanding fracture pattern or inhomogeneities like passage over the border between different rock types.

Acknowledgement

Tomofumi Koyama from the Royal Institute of Technology, Stockholm, carried out the

Particle Flow Code Analyses reported under Chapter 3.

Malin Johansson, Itasca Geomekanik AB, worked with the treatment and the visualization of the raw data, obtained from the numerical analyses. She also did extensive editing on the drafted text in order to conform the material into the layout required by SKB.

References

Itasca Consulting Group Inc., 2003. The distinct element program 3DEC.

Itasca Consulting Group Inc., 2004. Particle Flow Code (PFC^{2D}).

Mas Ivars D, Hakami, H, 2005. Effect of a sub-horizontal fracture zone and rock mass heterogeneity on the stress field in Forsmark area – A numerical study using 3DEC. Preliminary site description Forsmark area – version 1.2. SKB R-05-59, Svensk Kärnbränslehantering AB.

Sjöberg J, Lindfors U, Perman F, Ask D, 2005. Forsmark Site investigation: Evaluation of the state of stress at the Forsmark Site. SKB R-05-35, Svensk Kärnbränslehantering AB.

SKB, 2005. Preliminary site description. Forsmark area – version 1.2. SKB R-05-18, Svensk Kärnbränslehantering AB.

SKB, 2006. Site descriptive modelling Forsmark stage 2.1. Feedback for completion of the site investigation including input from safety assessment and repository engineering. SKB R-06-38. Svensk Kärnbränslehantering AB.

Appendix 1

Particle Flow Code (PFC) simulations

A1.1 Numerical calibration of microscopic mechanical parameters

A typical PFC^{2D} model requires the following micro-mechanical parameters for the system characterization: 1) particle radius, 2) stiffness of the particle contacts, 3) friction coefficient between particles and 4) normal and shear strength for bonds. Since these micro-mechanical parameters cannot be measured directly during laboratory experiments, numerical calibration is required to back-calculate them using measured values of some commonly measured intact rock properties, such as Young's modulus, Poisson's ratio and uniaxial compressive strength (UCS). Figure A1-1 shows a particle mechanics model of a Forsmark granite sample (of about 5 cm×12 cm in size) with 8,381 particles. The horizontal (upper and lower) boundaries were moved slowly to simulate the uniaxial compression test. The axial stress and strain are derived from the calculated contact forces and particle displacement, respectively, at the horizontal boundaries and selected reference particles respectively. During the calibration, to reduce the number of unknown microscopic parameters, the following assumptions were made: 1) minimum particle radius is fixed to 350 μm, which is assumed to represent grain size distribution of rock minerals when actual grain size distribution is not available, 2) all particle has the same density equal to the density of rock core sample measured during the laboratory experiment, 3) the values of Young's modulus for particle contact and parallel bond are set equal, 4) stiffness ratios of particle contact and parallel bond are set as the same, 5) both parallel bond and normal and shear strength were given deterministically, even though these values can be given stochastically.

Table A1-1 and Table A1-2 shows the list of the microscopic parameters adopted in this work to characterizing the microscopic behavior of the granite rock and the calibration results, respectively. The values for Young's modulus, Poisson's ratio and uniaxial compressive strength (UCS) used to calibrate the microscopic parameters, were obtained from the laboratory experiments and reported in the preliminary site description of the Forsmark area – version1.2 /SKB 2005/.

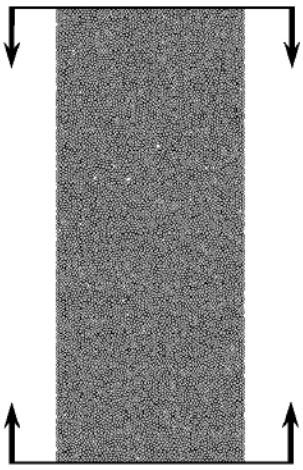

Figure A1-1. *The synthetic material of Forsmark granite with 8,381 particles and uniaxial compressive testing environment for PFC^{2D}.*

Table A1-1. Microscopic parameters of PFC^{2D} model used in this work.

PFC^{2D} model (domain size)	Lab. scale model (5×12 cm)	Field scale model (2,000×500 m)
Ball Density [kg/m^3]	2,650	2,650
Minimum ball radius, R_{min} [m]	3.5×10^{-4}	3.5
Ball size ratio, R_{max}/R_{min}	1.5	1.5
Number of balls	8,381	13,969
Ball-ball contact Young's modulus, E_c [GPa]	63	63
Ball stiffness ratio, k_n/k_s	2.5	2.5
Young's modulus of parallel bond, $\bar{E}_c$ [GPa]	63	63
Parallel bond stiffness ratio, λ	2.5	2.5
Particle friction coefficient, μ	0.5	0.5
Parallel bond normal strength, mean, $\bar{\sigma}_c$ [MPa]	302.5	302.5
Parallel bond normal strength, std. dev, $\bar{\sigma}_c$ [MPa]	0	0
Parallel bond shear strength, mean, $\bar{\tau}_c$ [MPa]	121	121
Parallel bond shear strength, std. dev, $\bar{\tau}_c$ [MPa]	0	0

Table A1-2. Calibration results.

	PFC^{2D} model	Lab. experiment
Sample size (Diameter [mm]/length [mm])	50/120	50/120
Young's modulus, E [GPa]	74.24	75
Poisson's ratio, v	0.241	0.24
Uniaxial compressive strength, q_u [MPa]	231.38	230

A1.2 PFC models for the sheet joint structure in Frsmark area

In this work, the following two geological structures were considered in the conceptual model; 1) a semi-detached discontinuity, which runs below the top rock containing the sheet joint structure, and 2) a preferred orientation at the grain size level, which should have occurred in the top rock horizon during the micro-tectonic activities in connection to the formation of that rock. Figure A1-6 shows the PFC model for the study area (2,000×500 m) with 13,969 particles and these two geological structures.

In the Table A1-1, the lists of the microscopic parameters adopted in both laboratory and field scale models in this work. It should be noted that the increase of minimum particle radius for field scale model is proportional to the domain size increase. The same value microscopic parameters were used for field scale model even though particle size was changed.

To investigate the effect of these structures on the mechanical behavior, six different model geometries were considered as shown in Figure A1-2 to Figure A1-7 and Table A1-3. There is no contact bondage along the semi-detached boundary (model geometry I), which means that the values of parallel bond in both normal and shear directions are zero and upper and lower rocks are detached completely. The weaker layer with different thickness was considered along the semi-detached boundary (from model geometry II to VI) and ten times weaker parallel bond values were given in this layer. The weaker mechanical properties, weaker parallel bond in both normal and shear directions, were also given along the preferred orientation in the top rock with different intervals (from model geometry IV to VI). The following two different weakening values for the parallel bond along the preferred orientation were considered; 1) one half and 2) one fifth, called Case I and II, respectively. Table A1-4 shows the list of the microscopic parameters for the weak layers along the semi-detached boundary and preferred orientation.

Table A1-5 also shows the calculated Young's modulus, Poisson's ratio and uniaxial compressive strength (UCS) using weakening values for the weak layers along the semi-detached boundary and preferred orientation. When smaller parallel bond strength was given, the uniaxial compressive strength of the rock becomes also smaller proportionally.

The following two different types of boundary conditions were considered; a) superficial crustal shortening, where the vertical walls moves translational with a constant velocity and b) superficial crustal shortening with a rotational component, where the vertical walls rotate with a constant angular velocity. The displacement in y-direction was fixed at the bottom. Figure A1-11 show the boundary conditions applied in this study.

Table A1-3. The description of six different model geometries for the Forsmark area.

Model geometry	Geological structure
I	A semi-detached discontinuity at the depth of 250 m
II	A semi-detached discontinuity with 17.5 m thickness at the depth of 250 m
III	A semi-detached discontinuity with 35 m thickness at the depth of 250 m
IV	A semi-detached discontinuity with 35 m thickness at the depth of 250 m and one preferred orientation with 17.5 m thickness in the middle of the top rock.
V	A semi-detached discontinuity with 35 m thickness at the depth of 250 m and two preferred orientations with 17.5 m thickness and at the interval of 83 m in the top rock.
VI	A semi-detached discontinuity with 35 m thickness at the depth of 250 m and two preferred orientations with 17.5 m thickness and at the interval of 62.5 m in the top rock.

Table A1-4. Microscopic parameters for semi-detached boundary and preferred orientation.

PFC^{2D} model (domain size)	Semi-detached boundary	Preferred oriantation Case I	Case II
Ball Density [kg/m^3]	2,650	2,650	2,650
Minimum ball radius, R_{min} [m]	3.5	3.5	3.5
Ball size ratio, R_{max}/R_{min}	1.5	1.5	1.5
Ball-ball contact Young's modulus, E_c [GPa]	63	63	63
Ball stiffness ratio, k_n/k_s	2.5	2.5	2.5
Young's modulus of parallel bond, $\bar{E}_c$ [GPa]	63	63	63
Parallel bond stiffness ratio, λ	2.5	2.5	2.5
Particle friction coefficient, μ	0.5	0.5	0.5
Parallel bond normal strength, mean, $\bar{\sigma}_c$ [MPa]	30.25	151.25	60.5
Parallel bond normal strength, std. dev, $\bar{\sigma}_c$ [MPa]	0	0	0
Parallel bond shear strength, mean, $\bar{\tau}_c$ [MPa]	12.1	60.5	24.2
Parallel bond shear strength, std. dev, $\bar{\tau}_c$ [MPa]	0	0	0

Table A1-5. Calculated Young's modulus, Poisson's ration and uniaxial compressive strength in the semi-detached boundary and preferred orientation.

	Semi-detached boundary	Preferred orientation Case I	Case II
Sample size (Diameter [mm]/length [mm])	50/120	50/120	50/120
Young's modulus, E [GPa]	79.9	74.18	75.3
Poisson's ratio, v	0.217	0.238	0.236
Uniaxial compressive strength, q_u [MPa]	20.57	93.22	39.57

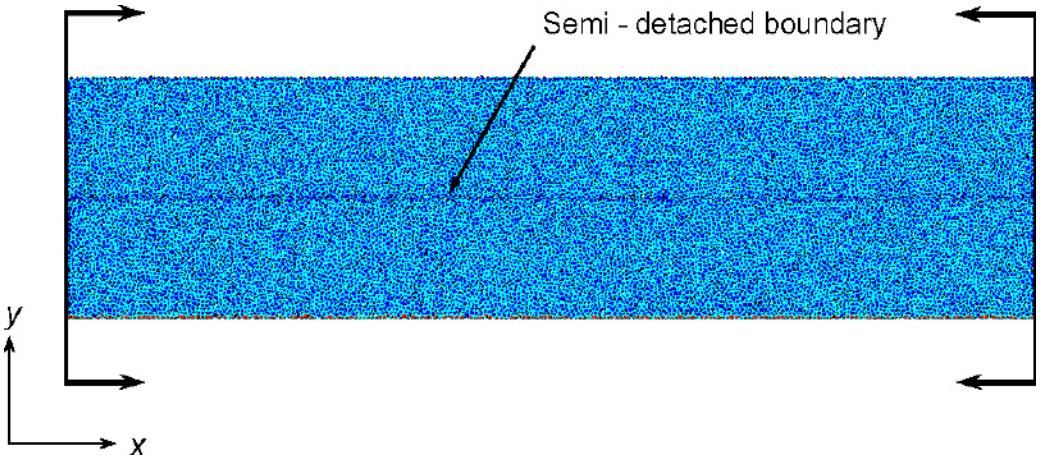

Figure A1-2. *PFC model I – geometry and boundary conditions.*

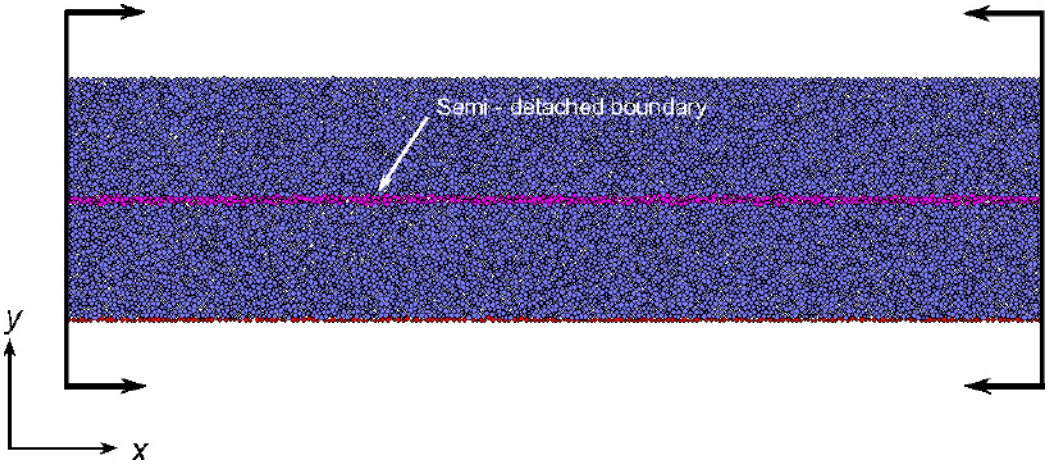

Figure A1-3. *PFC model II – geometry and boundary conditions.*

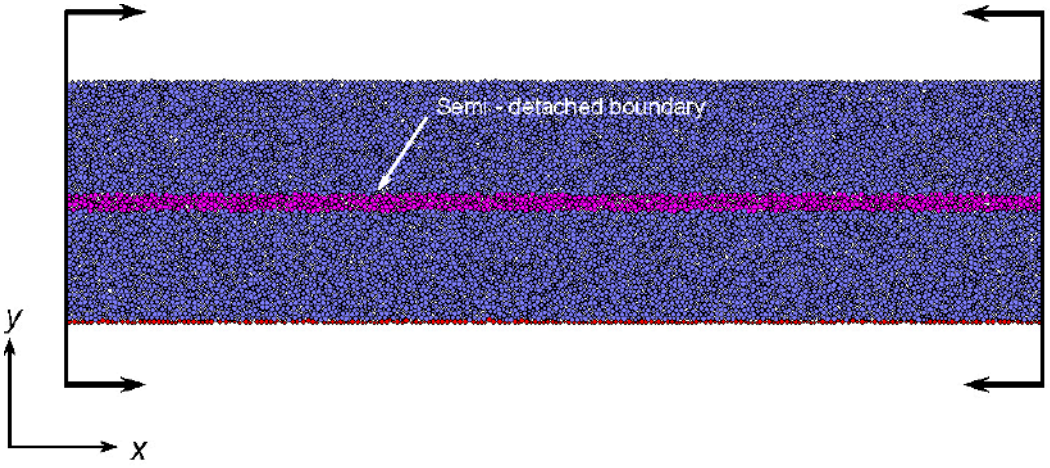

Figure A1-4. *PFC model III – geometry and boundary conditions.*

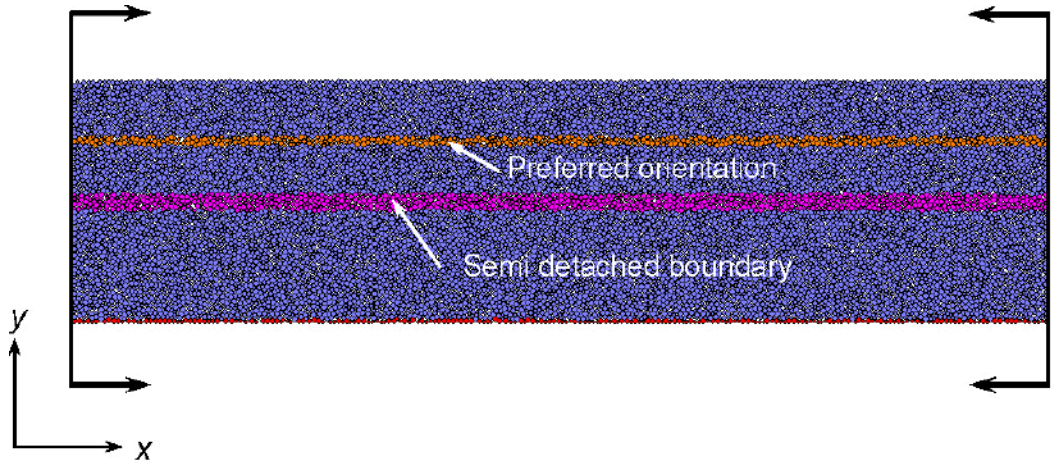

Figure A1-5. *PFC model IV – geometry and boundary conditions.*

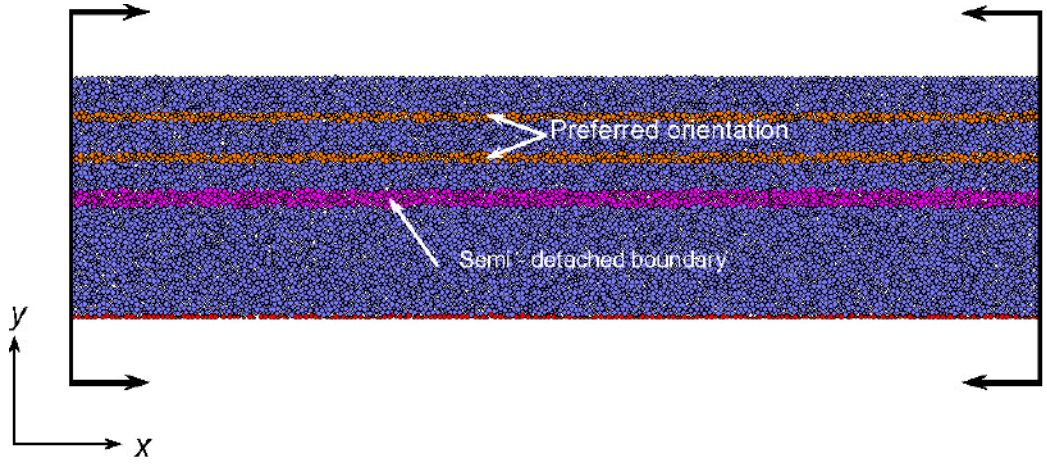

Figure A1-6. *PFC model V – geometry and boundary conditions.*

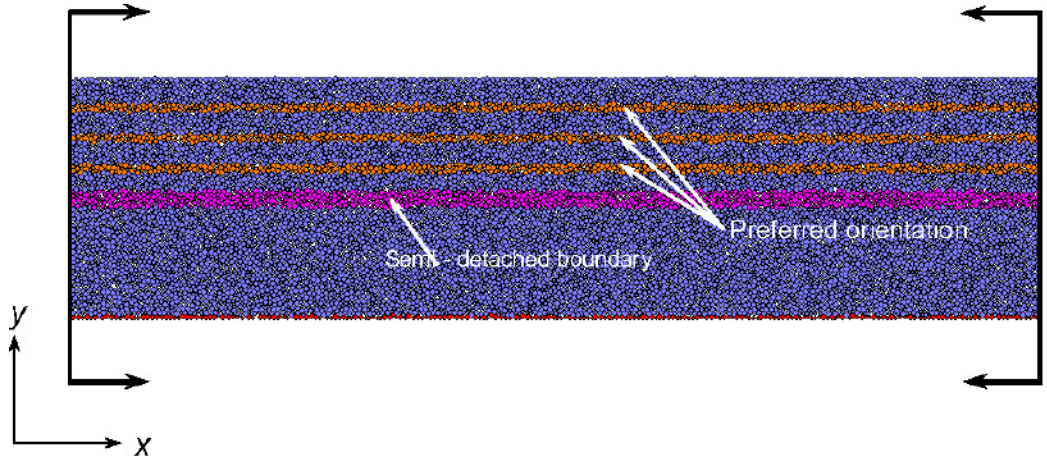

Figure A1-7. *PFC model VI – geometry and boundary conditions.*

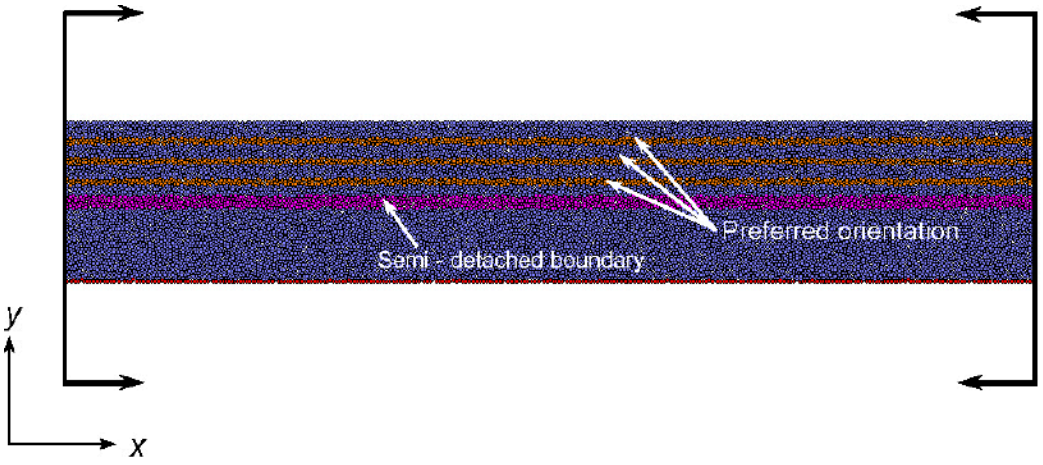

Figure A1-8. *PFC model VI_wide – geometry and boundary conditions.*

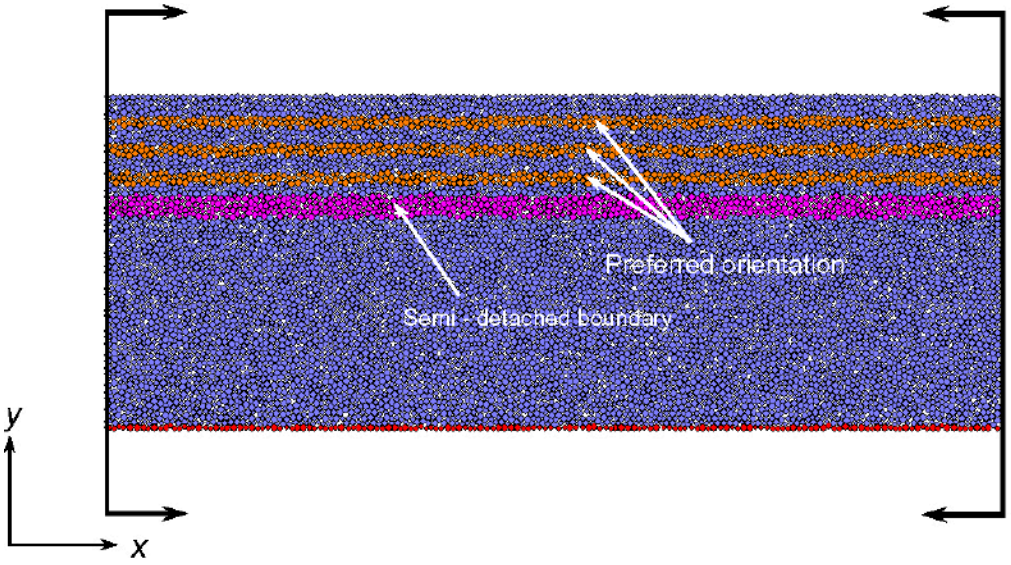

Figure A1-9. *PFC model V_deep (750) – geometry and boundary conditions.*

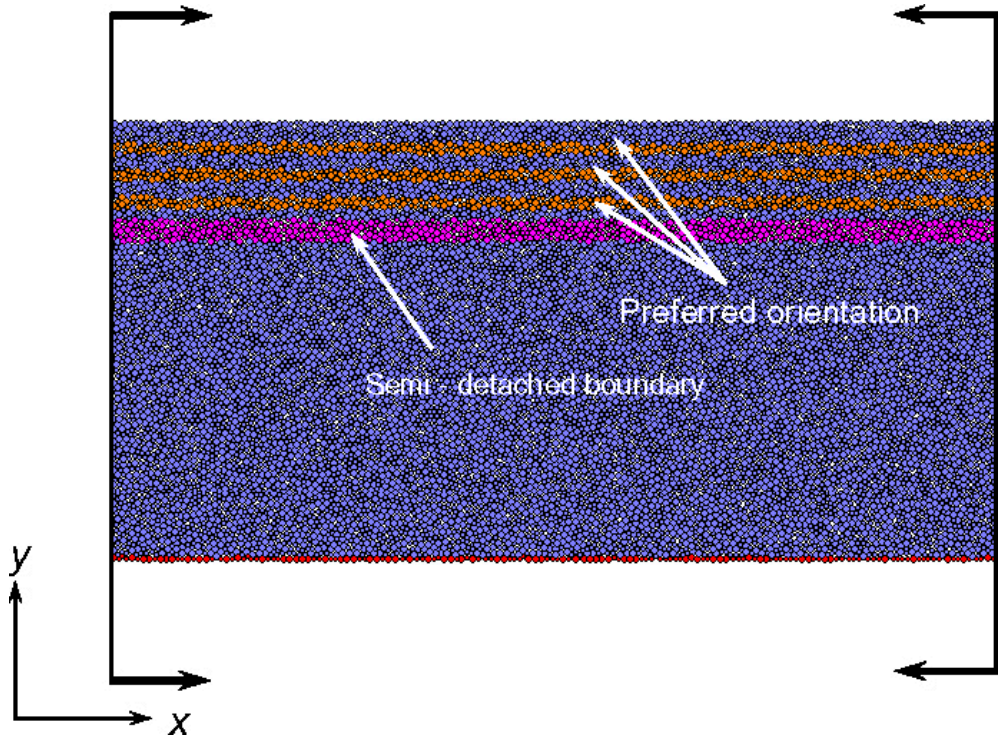

Figure A1-10. *PFC model VI_deep (1,000) – geometry and boundary conditions.*

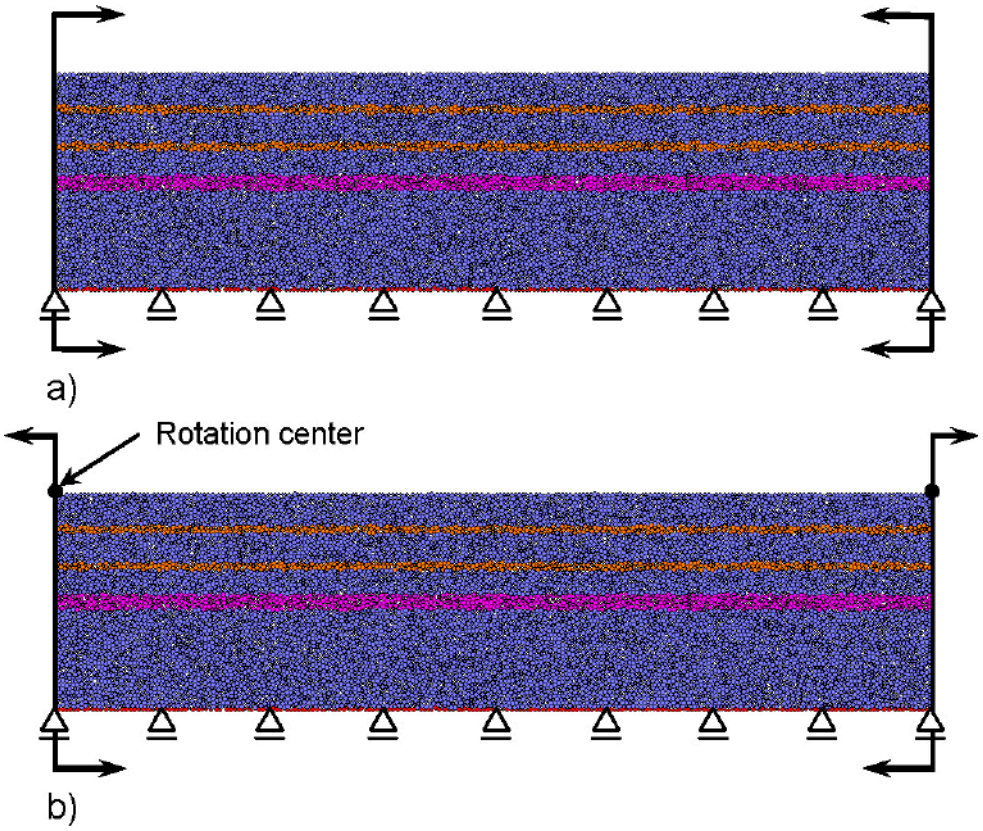

Figure A1-11. *Two different types of stress boundary conditions; a) superficial crustal shortening and b) superficial crustal shortening with a rotational component.*

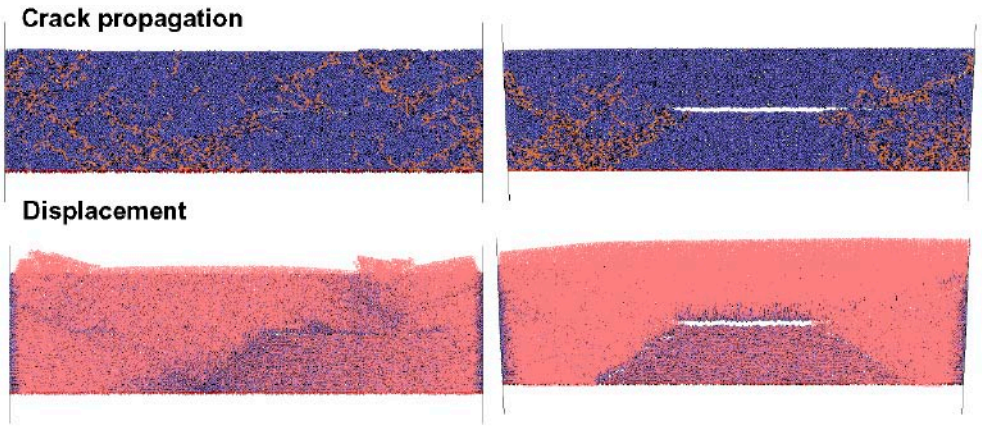

Figure A1-12. *PFC model I – simulation results.*

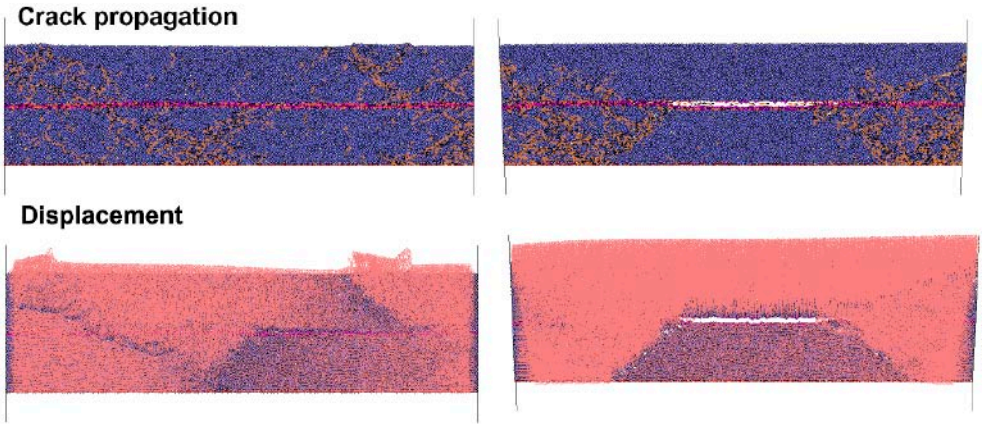

Figure A1-13. *PFC model II – simulation results.*

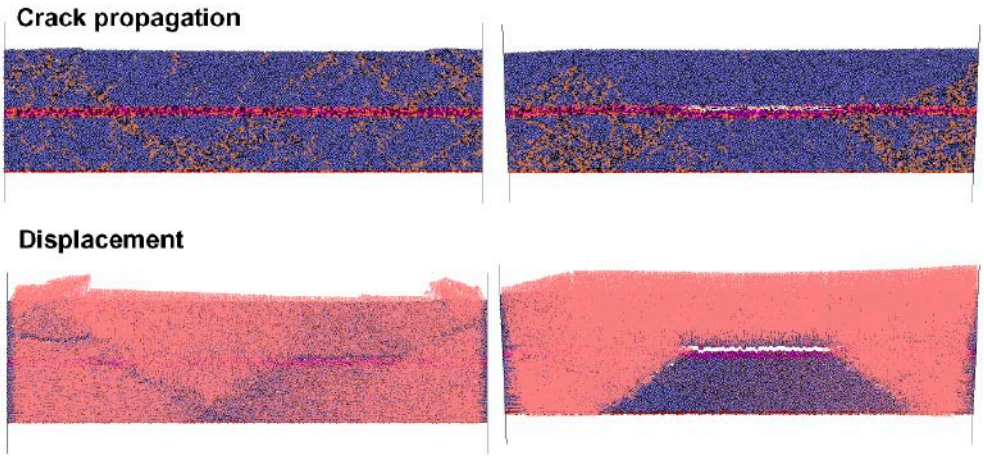

Figure A1-14. *PFC model III – simulation results.*

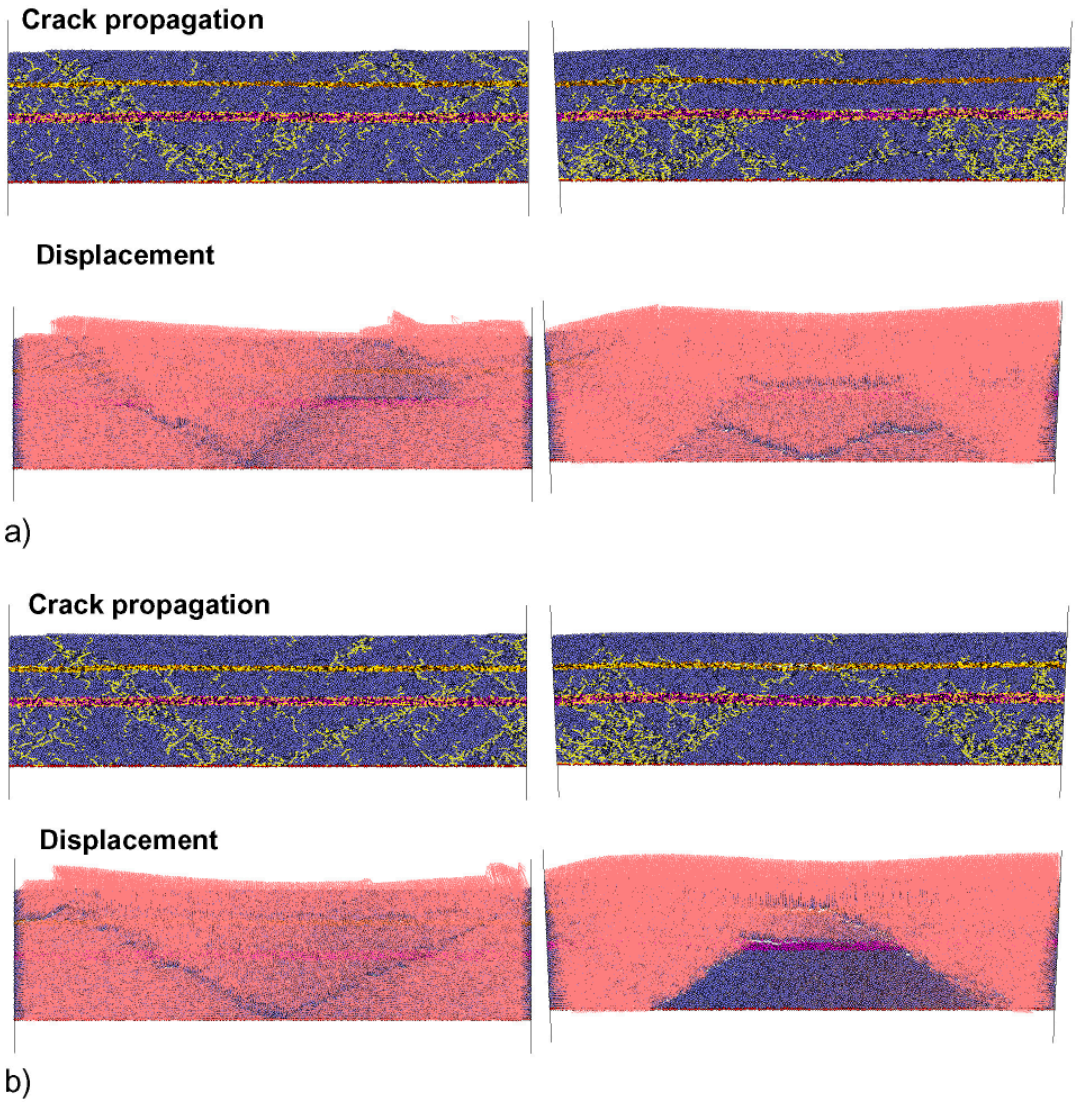

Figure A1-15. *PFC model IV – simulation results; a) case 1 and b) case 2.*

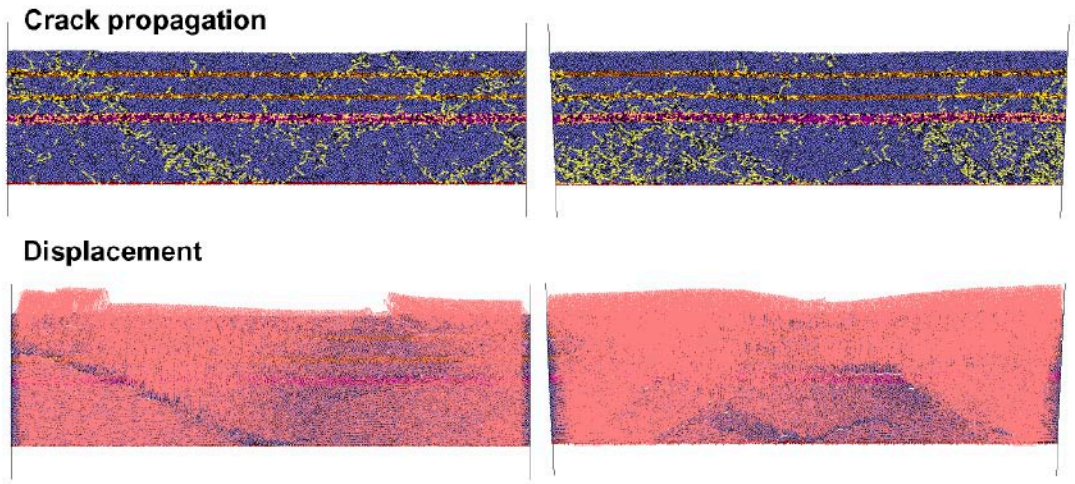

a)

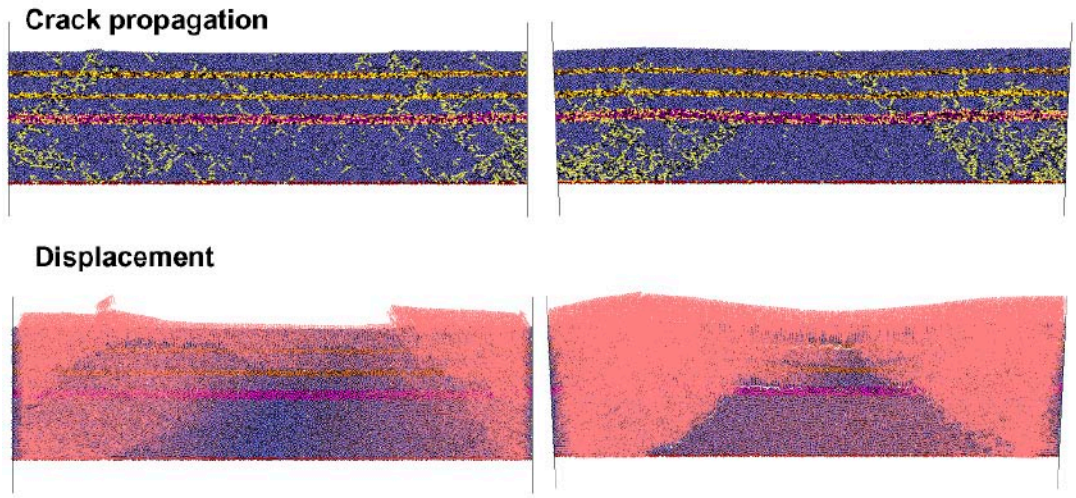

b)

Figure A1-16. *PFC model V – simulation results; a) case 1 and b) case 2.*

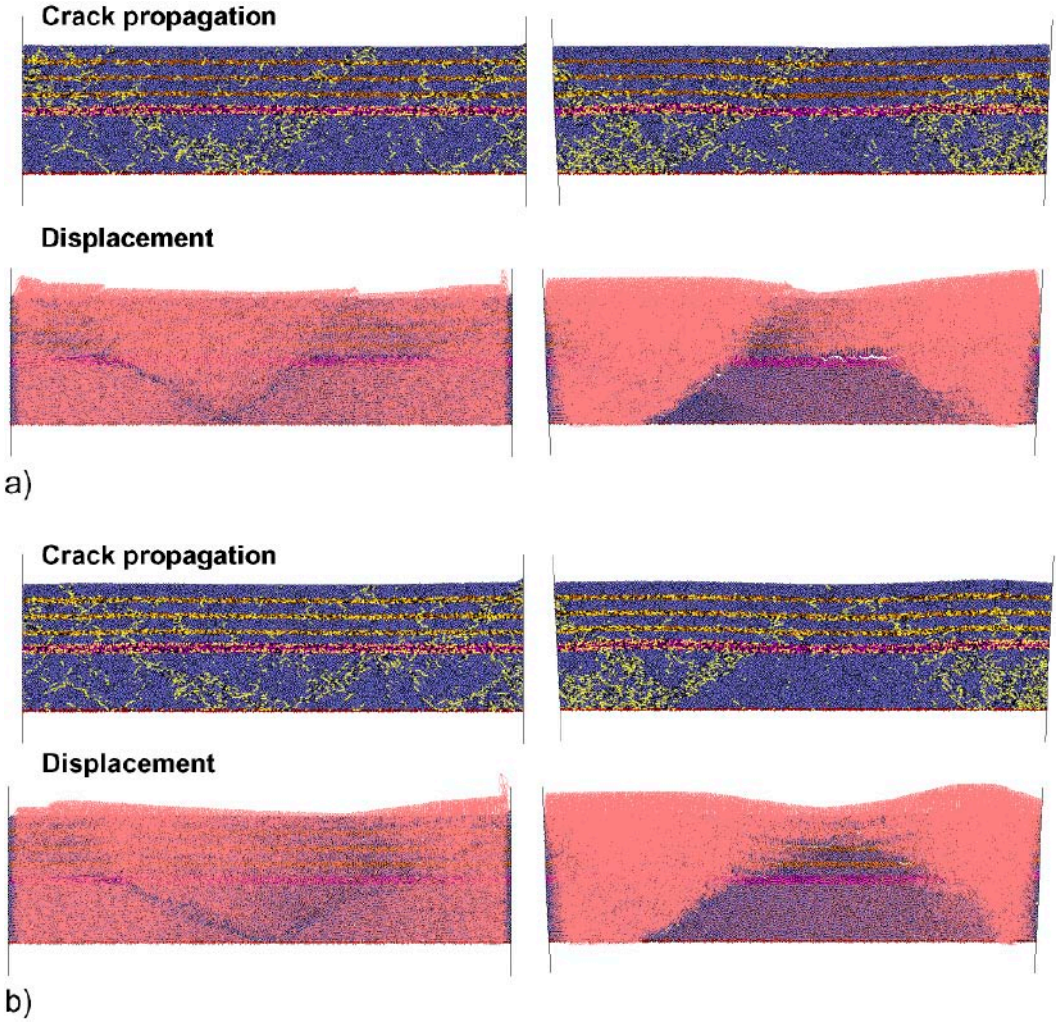

Figure A1-17. *PFC model VI – simulation results; a) case 1 and b) case 2.*

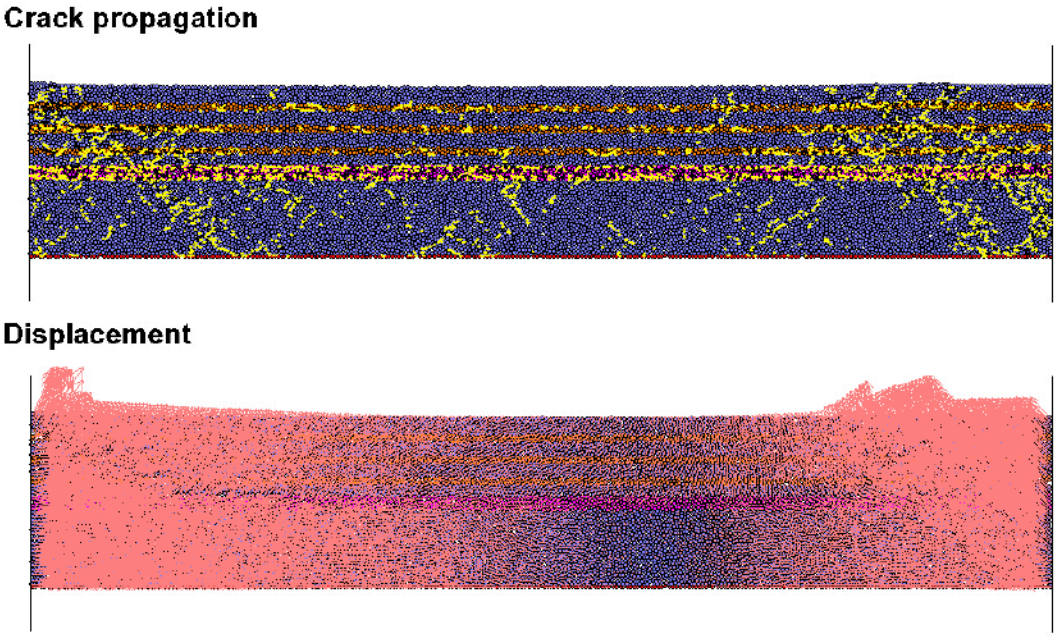

Figure A1-18. *PFC model VI_wide – simulation results.*

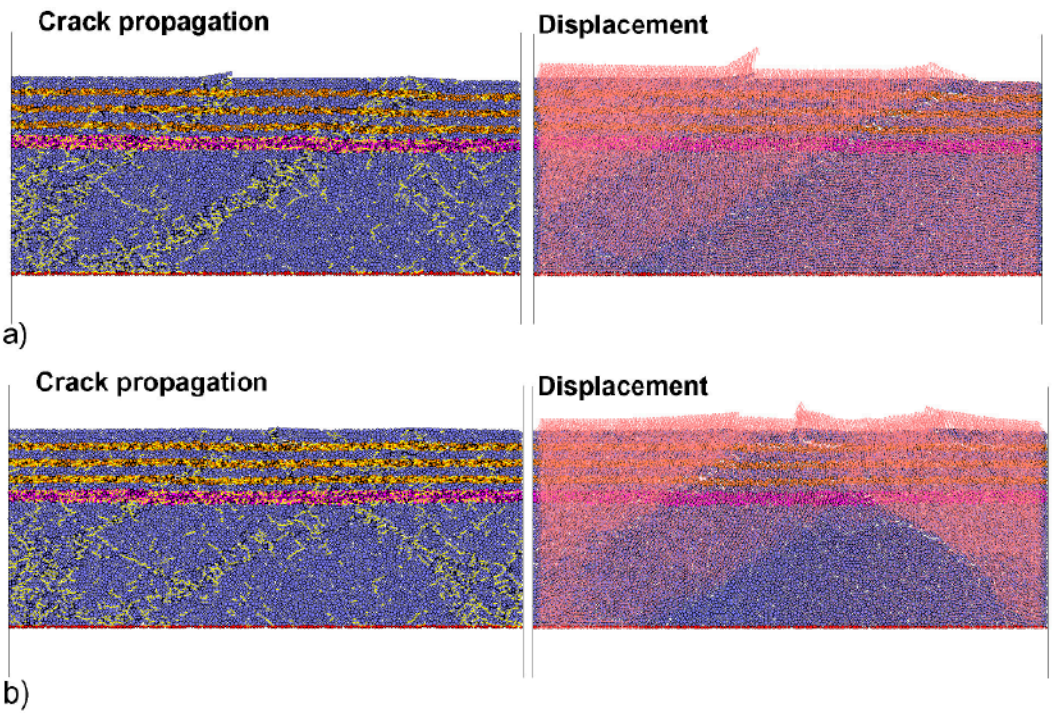

Figure A1-19. *PFC model VI_deep (750) – simulation results; a) case 1 and b) case 2.*

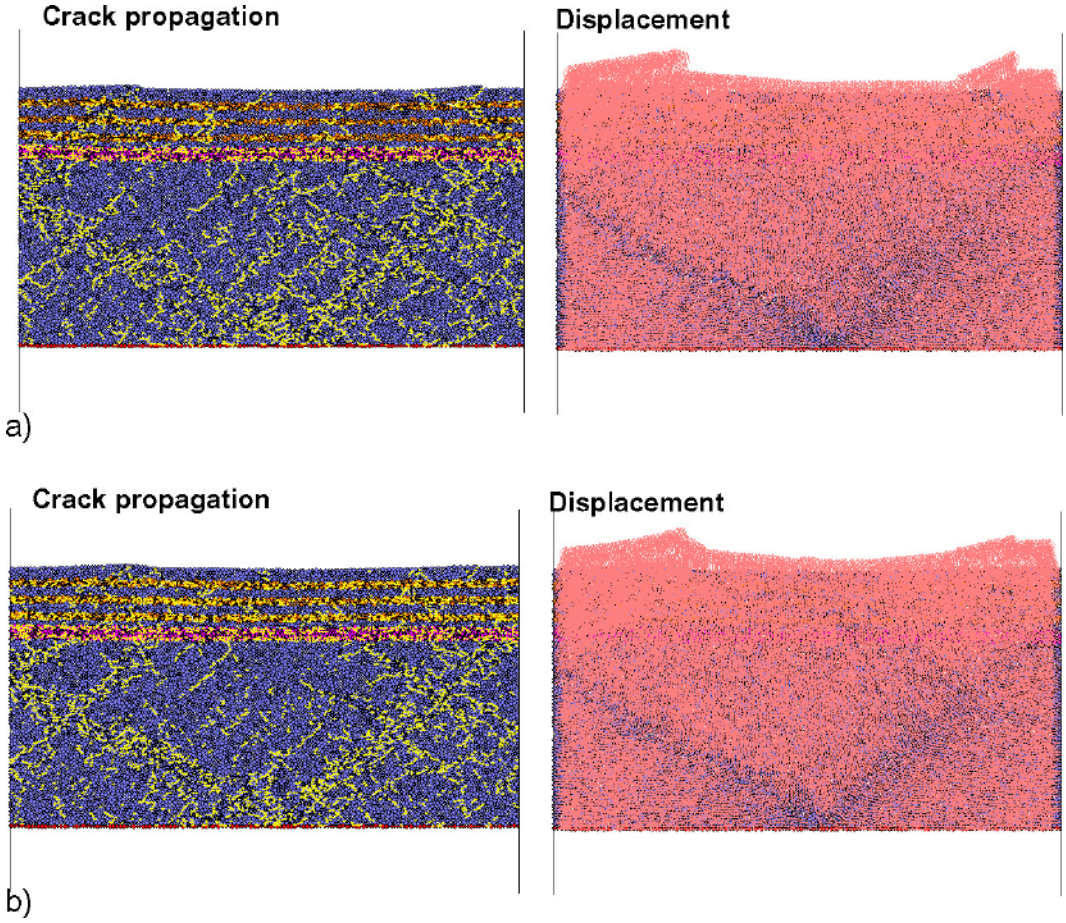

Figure A1-20. *PFC model VI_deep (1,000) – simulation results; a) case 1 and b) case 2).*

Appendix 2

Regional model – The computed variations of the in situ stress field from the 3DEC analyses

Stresses

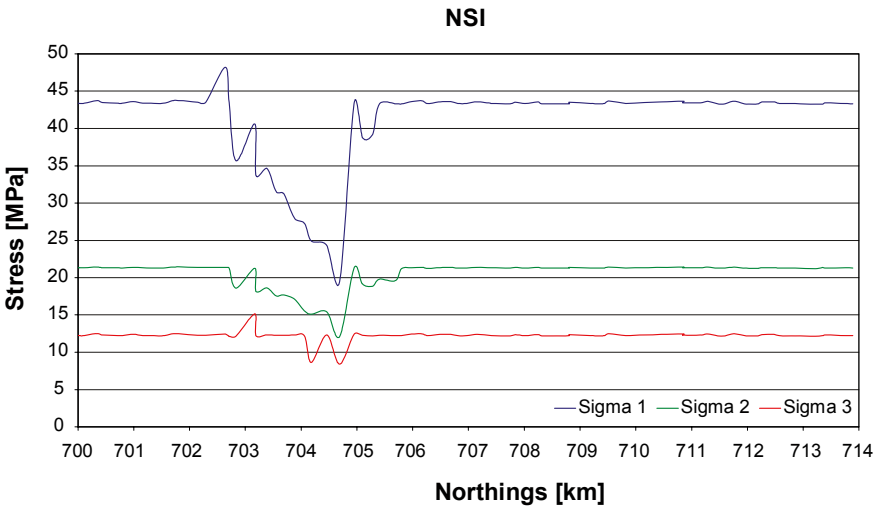

Figure A2-1. *Variation of σ_1, σ_2 and σ_3 along N–S scan line at 400 m depth.*

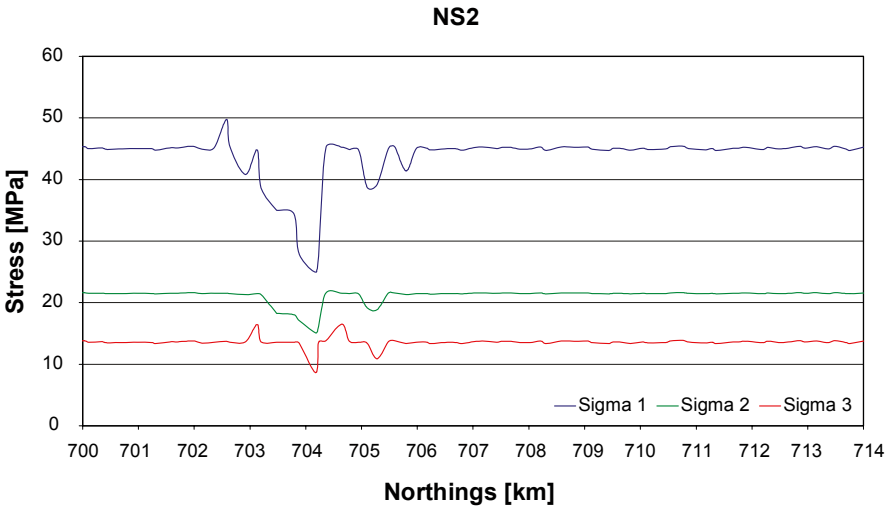

Figure A2-2. *Variation of σ_1, σ_2 and σ_3 along N–S scan line at 500 m depth.*

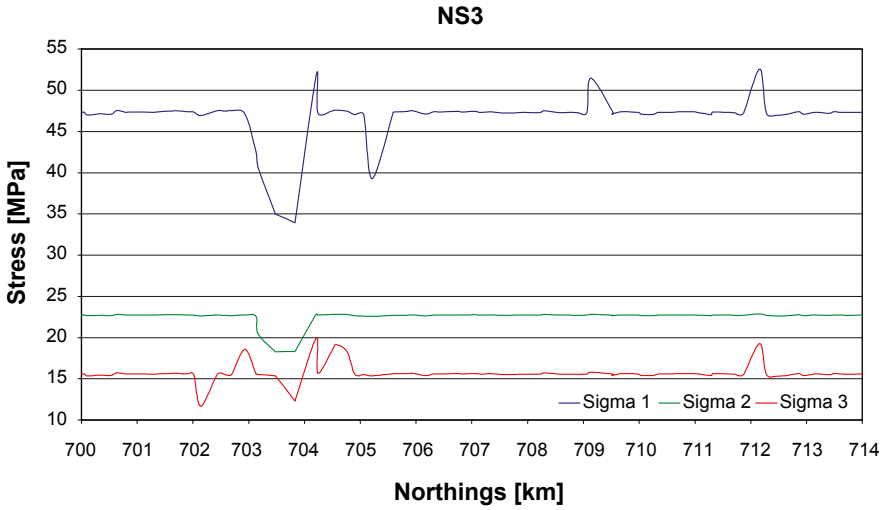

Figure A2-3. *Variation of σ_1, σ_2 and σ_3 along N–S scan line at 600 m depth.*

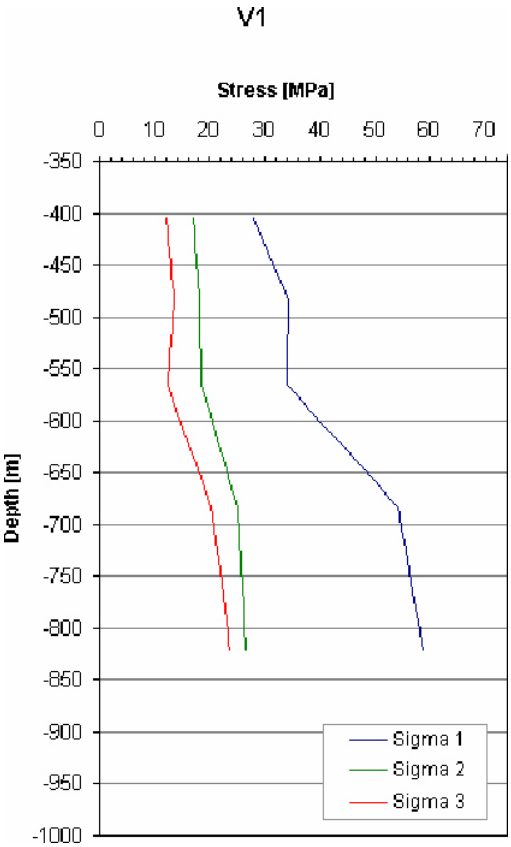

Figure A2-4. *Variation of σ_1, σ_2 and σ_3 along the vertical scan line, the position is shown on Figure 4-8.*

Trends

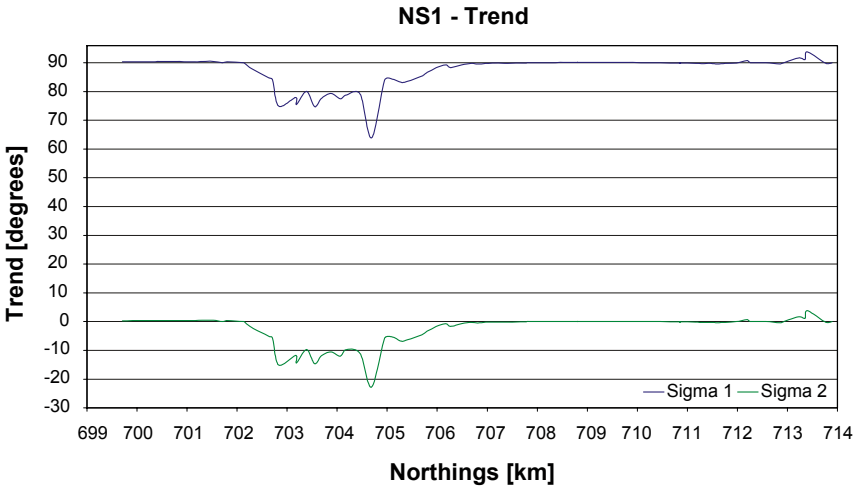

Figure A2-5. *Variation in trend of σ_1 and σ_2 along N–S scan line at 400 m depth.*

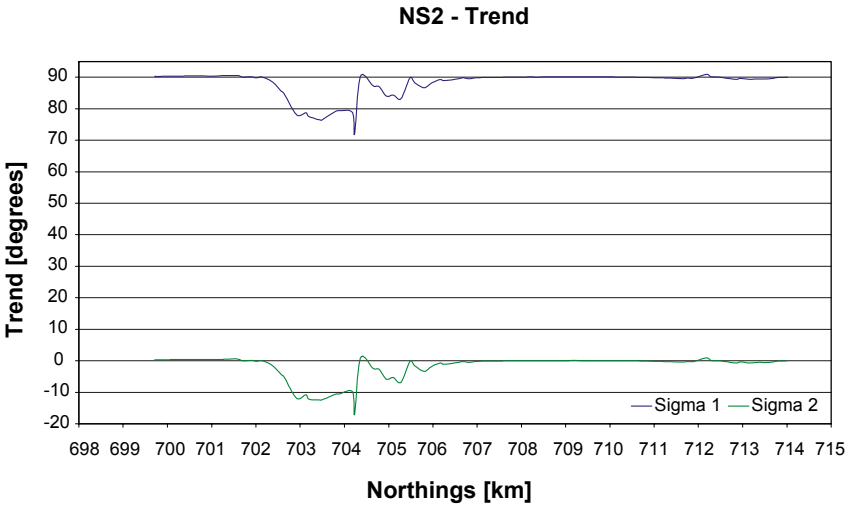

Figure A2-6. *Variation in trend of σ_1 and σ_2 along N–S scan line at 500 m depth.*

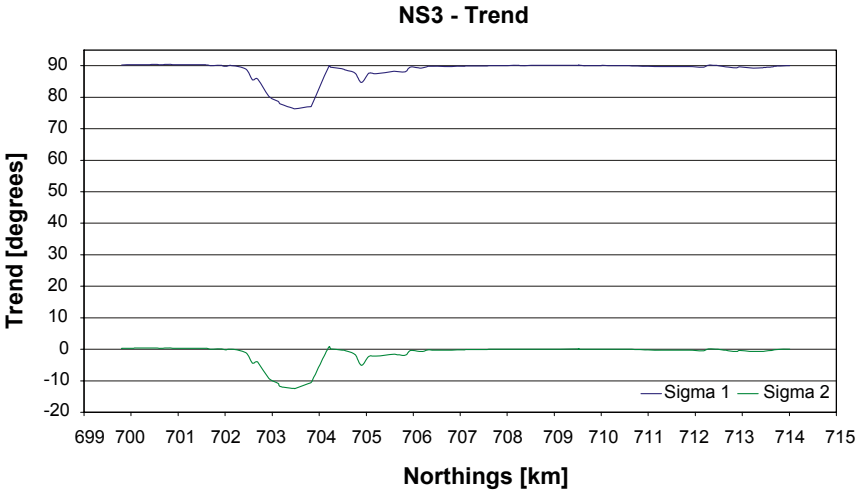

Figure A2-7. *Variation in trend varies of σ_1 and σ_2 along the N–S scan line at 600 m depth.*

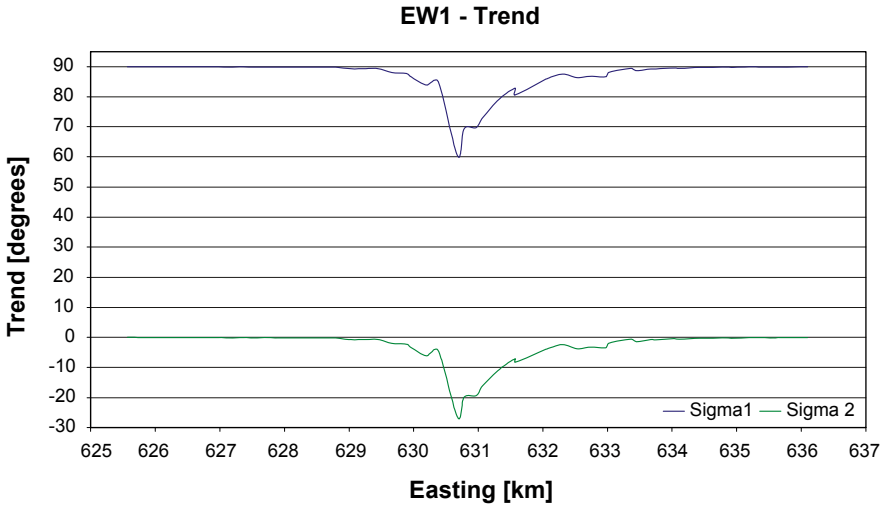

Figure A2-8. *Variation in trend of σ_1 and σ_2 along the E–W scan line at 400 m depth.*

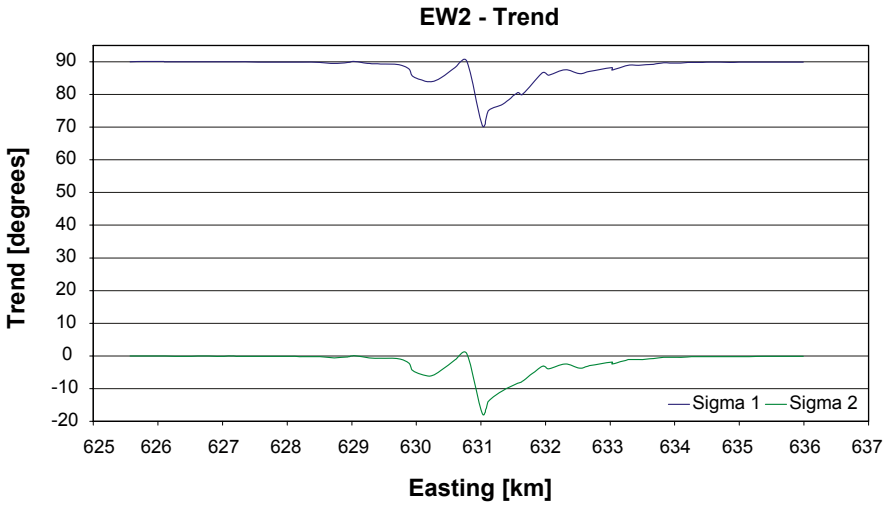

Figure A2-9. *Variation in trend of σ_1 and σ_2 along E–W scan line at 500 m depth.*

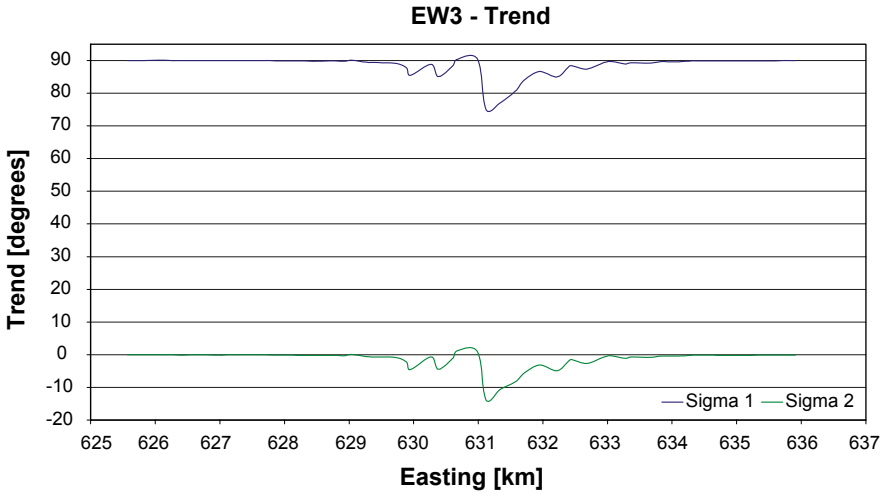

Figure A2-10. *Variation in trend of σ_1 and σ_2 along the E–W scan line at 600 m depth.*

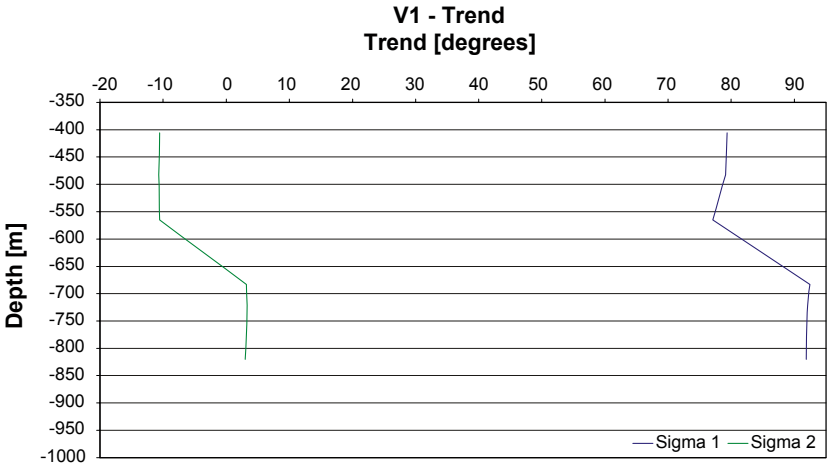

Figure A2-11. *Variation in trend of σ_1 and σ_2 along the vertical scan line, the position is shown on Figure 4-8.*

Plunge

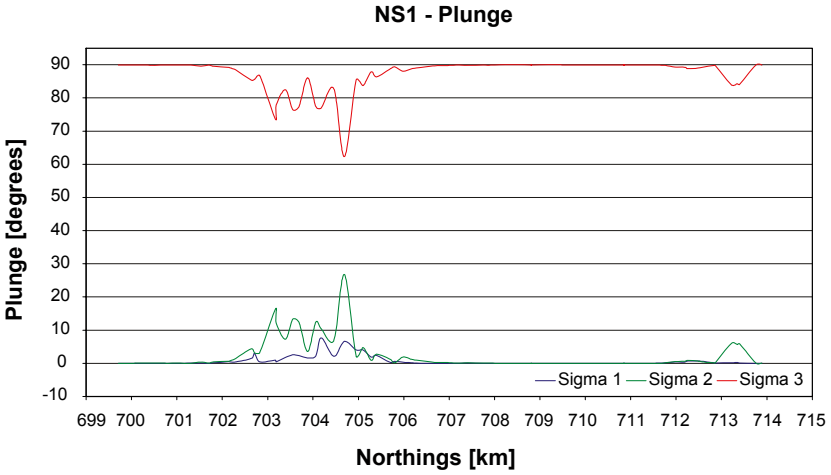

Figure A2-12. *Variation in plunge of σ_1, σ_2 and σ_3 along N–S scan line at 400 m depth.*

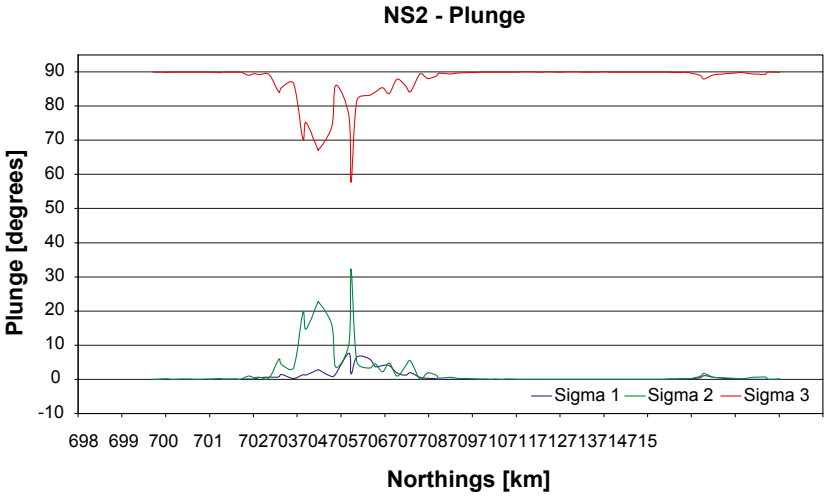

Figure A2-13. *Variation in plunge of σ_1, σ_2 and σ_3 along N–S scan line at 500 m depth.*

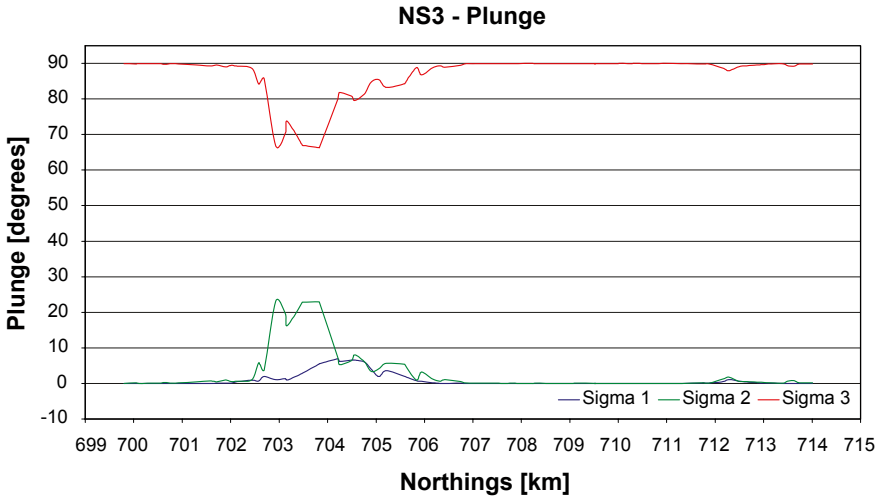

Figure A2-14. *Variation in plunge of σ_1, σ_2 and σ_3 along N–S scan line at 600 m depth.*

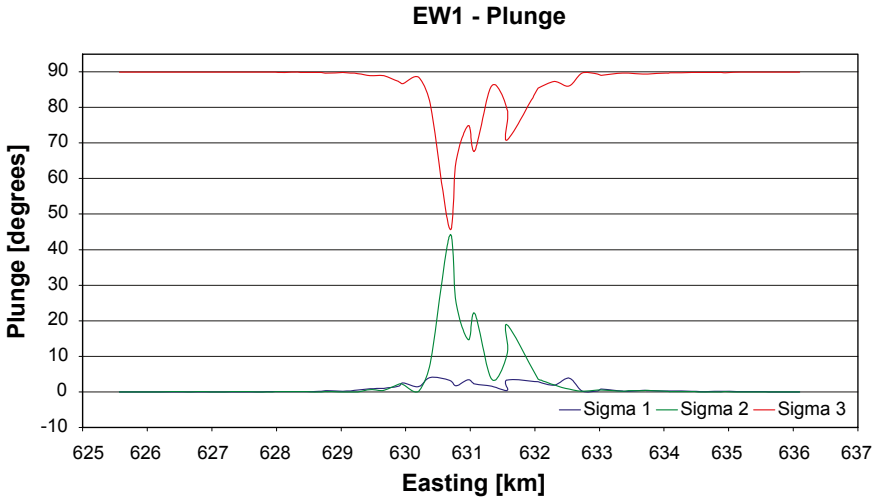

Figure A2-15. *Variation in plunge of σ_1, σ_2 and σ_3 along E–W scan line at 400 m depth.*

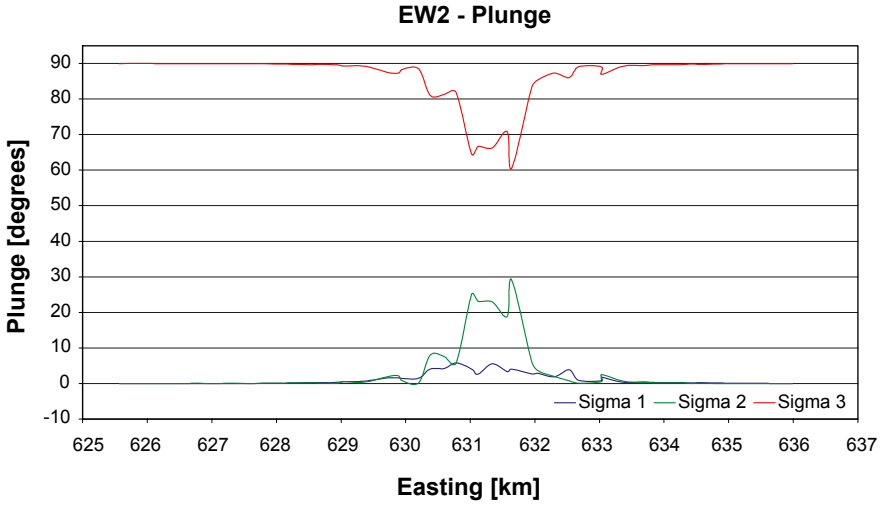

Figure A2-16. *Variation in plunge of σ_1, σ_2 and σ_3 along E–W scan line at 500 m depth.*

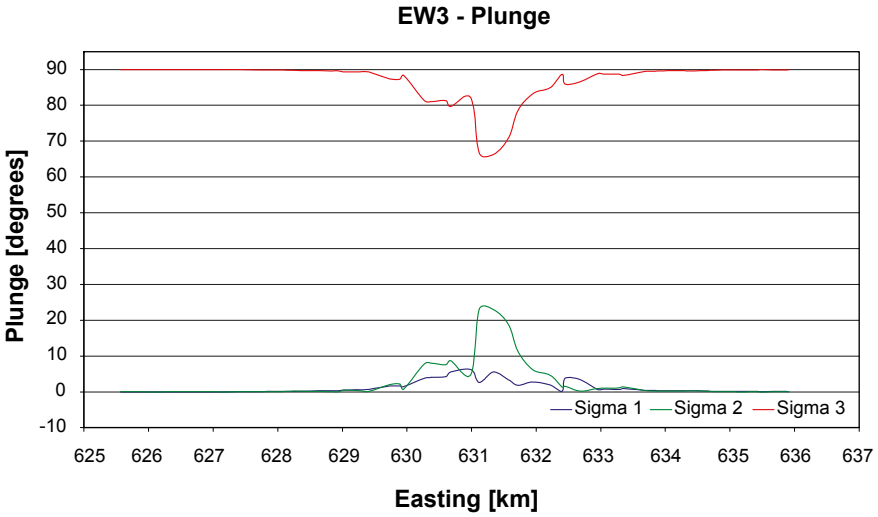

Figure A2-17. *Variation in plunge of σ_1, σ_2 and σ_3 along E–W scan line at 600 m depth.*

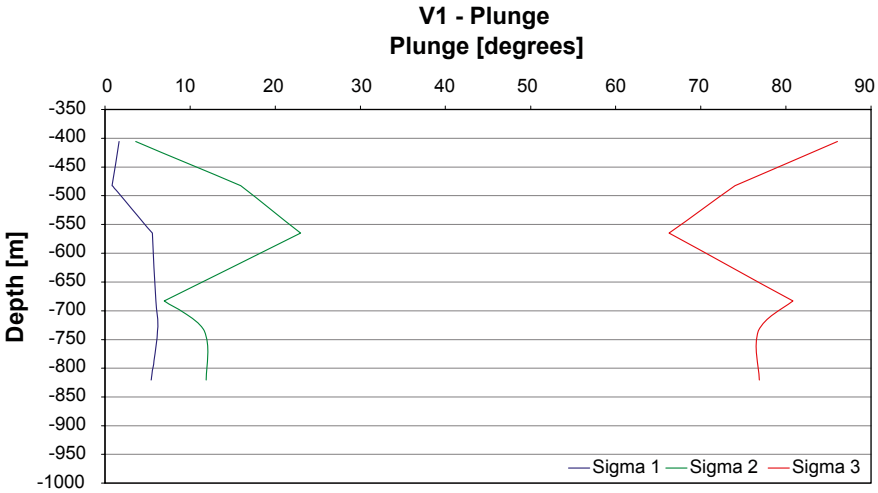

Figure A2-18. *Variation in plunge of σ_1, σ_2 and σ_3 along the vertical scan line, the position is shown on Figure 4-8.*